We are IntechOpen,
the world's leading publisher of
Open Access books
Built by scientists, for scientists

4,800
Open access books available

122,000
International authors and editors

135M
Downloads

Our authors are among the

154
Countries delivered to

TOP 1%
most cited scientists

12.2%
Contributors from top 500 universities

CLARIVATE ANALYTICS
BOOK CITATION INDEX
INDEXED

WEB OF SCIENCE™

Selection of our books indexed in the Book Citation Index
in Web of Science™ Core Collection (BKCI)

Interested in publishing with us?
Contact book.department@intechopen.com

Numbers displayed above are based on latest data collected.
For more information visit www.intechopen.com

5

Design of a Very Small Antenna for Metal-Proximity Applications

Yoshihide Yamada
National Defence Academy, Dept. of Electronic Engineering
Japan

1. Introduction

A radio frequency identification (RFID) system consists of a reader, a writer, and a tag. Film-type half-wavelength dipole antennas (shown in Fig. 1.1) have been used as tag antennas in many applications [1]. The antenna performance is governed by the electric current in the tag. When the abovementioned antenna is mounted on the surface of a metallic object, the radiation characteristics are seriously degraded because of the image current induced in the object. Therefore, studies have been carried out to construct tag antennas that are suitable for use with metallic objects, and some promising antenna types have been proposed.

In this chapter, design approaches for metal-proximity antennas (antennas placed in close proximity to a metal plate) are discussed. In Section 2, typical metal-proximity antennas are described. An example of the aforementioned type of antenna is a normal-mode helical antenna (NMHA), which can show high efficiency despite its small size. We focus on the design of this antenna. In Section 3, the fundamental equations used in the NMHA design are summarized. In particular, we propose an important equation for determining the self-resonant structure of the antenna. We fabricate an antenna to show that its electrical characteristics are realistic. In Section 4, we explain the impedance-matching method necessary for the NMHA and provide a detailed description of the tap feed. In Section 5, we discuss the use of NMHA as a tag antenna and provide the read ranges achieved.
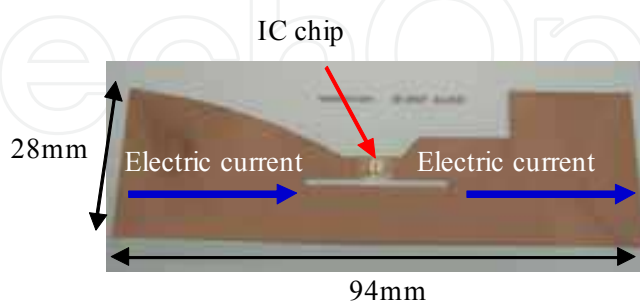

Fig. 1.1 A typical tag antenna

2. Tag antennas for metal-proximity use

Typical examples of metal-proximity tag antennas are given in Table 2.1. Some examples of metal-proximity antennas are patch antennas [2] and slot antennas [3], which can be

mounted on a metal plate. Since these antennas comprise flat plates, the antenna thickness decreases but the size does not small. Another example of a metal-proximity antenna is the normal-mode helical antenna (NMHA) [4]. The wire length of this antenna is approximately one-half of the wavelength, and hence, the antenna is small-sized. Moreover, because this antenna has a magnetic current source, it can be mounted on a metallic plate. The antenna gain increases when the antenna is placed in the vicinity of a metal plate. Because the antenna input resistance is small, a tap-feed structure is necessary to increase the resistance.
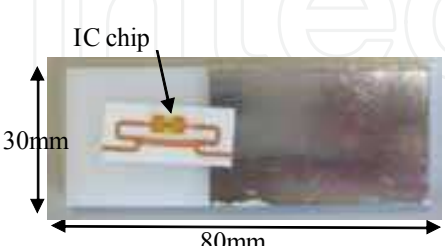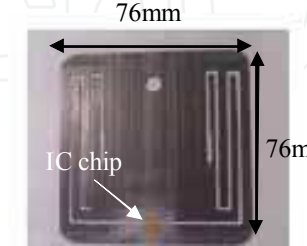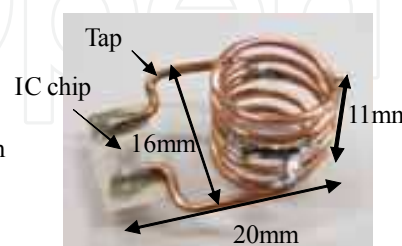
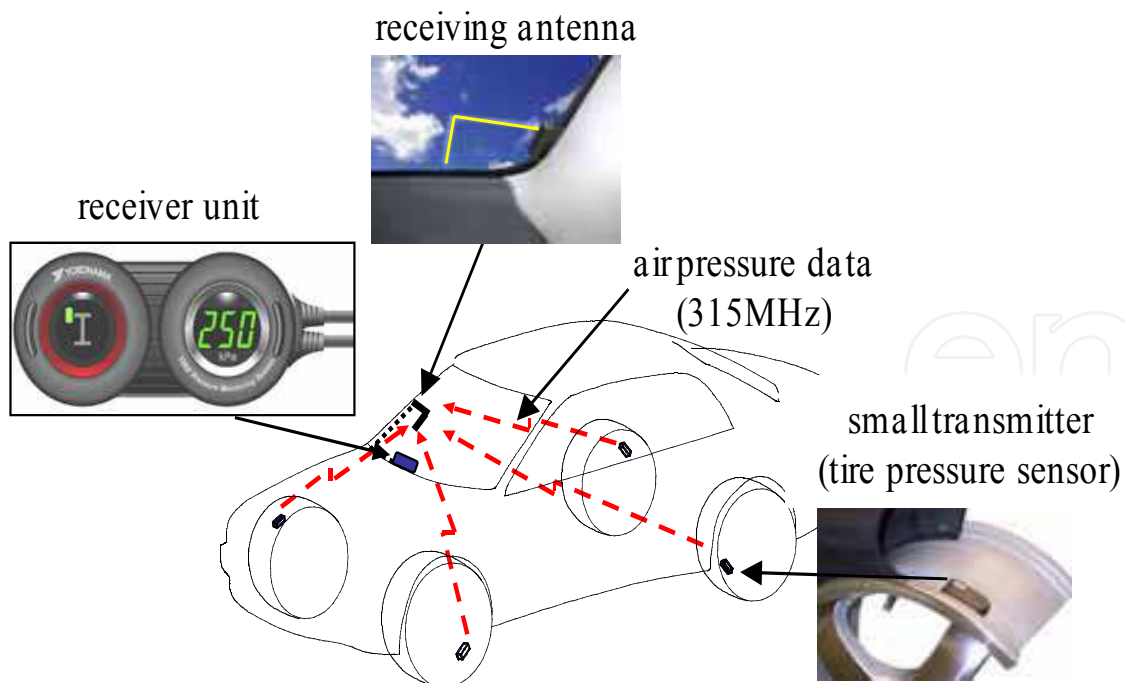|		
·Frequency 953MHz ·Thickness : 4mm ·Read range :13m ·Commercial products	·Frequency 915MHz ·Thickness : 0.25mm ·Read range 5m ·Researching	·Frequency 953MHz ·Thickness : 16mm ·Read range 8m ·Researching
[2] Patch antenna	[3] Slot antenna	[4] Normal mode helical antenna

Table 2.1 Metal-proximity tag antennas

Fig. 2.1 Application of NMHA to tire-pressure monitoring system

The feasibility of using very small NMHAs in a tire-pressure monitoring system (TPMS) [5] and metal-proximity RFID tags [6] has been studied. The RFID applications are explained in

detail in Section 5. Figure 2.1 shows the TPMS system (called AIRwatch) developed by The Yokohama Rubber Co., Ltd. Transmitters connected to tire-pressure sensors are mounted on the wheels, and a receiver unit is placed on the dashboard. A receiving antenna (a film antenna) is attached to the windshield. Each sensor uses the FSK scheme to modulate 315-MHz continuous waves with air pressure data. The modulated waves are transmitted from a small loop antenna in the sensor. The receiving antenna collects all the transmitted waves, and the pressure levels are indicated on the receiver unit. To apply this system to trucks and buses, it is necessary to replace the small-loop antenna with an NMHA [7] since the gain and effectiveness of the latter are high under metal-proximity conditions.

3. Design and electrical characteristics of normal-mode helical antenna

3.1 Features of NMHA

The structural parameters of the NMHA are shown in Fig. 3.1. The length, diameter, and number of turns of the antenna are denoted by H, D, and N, respectively. The diameter of the antenna wire is denoted by d. A comprehensive treatment of this antenna has been given by Kraus [8]. In Kraus's study, the antenna current was divided across the straight part and circular parts of the antenna. Conceptual expressions for the two current sources are shown in Fig. 3.1. The straight part acts like a small dipole antenna, and the circular parts act like small loop antennas. The radiation characteristics of these small loops are equivalent to those of a small magnetic current source. Therefore, the radiated electric fields are composed of two orthogonal electrical components produced by electric and magnetic current sources. Hence, the radiated electric field polarization becomes circular or elliptical depending on the H-to-D ratio. Because the radiated fields are produced by small electrical and magnetic current sources, the radiation patterns are almost constant for various small antennas. The directional gain is almost 1.5 (1.8 dBi).
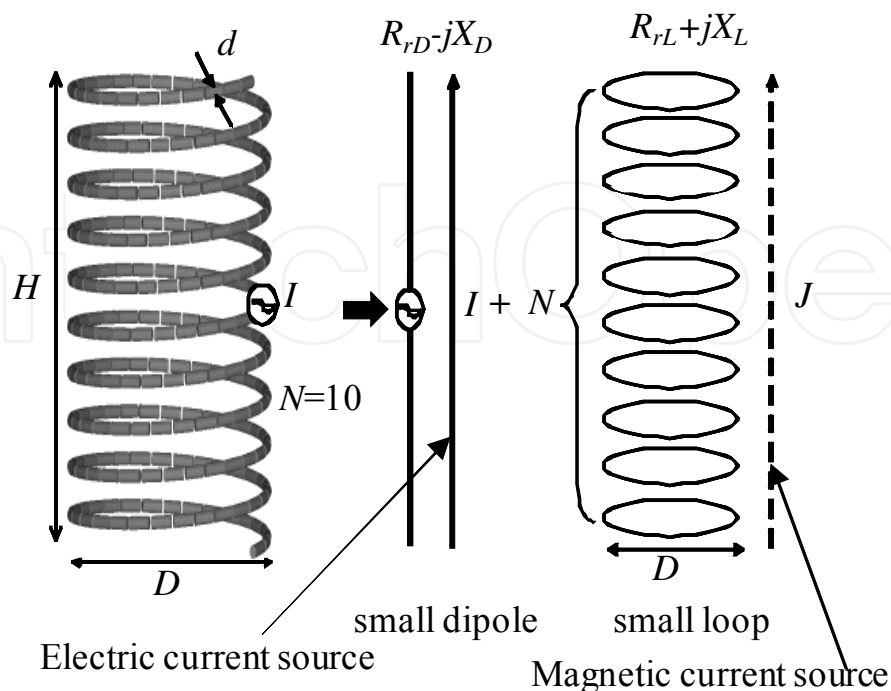

Fig. 3.1 Conceptual equivalence of normal-mode helical antenna

The existence of a magnetic current source is advantageous for using an antenna in the proximity of a metal plate. The electrical image theory indicates that radiation from a magnetic current source is increased by the existence of a metal plate. Another important feature of an NMHA is its impedance. A small dipole has capacitive reactance, and the small loops have inductive reactance. By appropriate choice of the *H, D,* and *N* values, the capacitive and inductive reactances can be made to cancel out each other. This condition is called the self-resonant condition, and it is important for efficient radiation production. In this case, the input impedance becomes a pure resistance. It should be noted that this pure resistance is small, and therefore, an impedance-matching structure is necessary. Moreover, the ohmic resistance of the antenna wire must be reduced to a considerable extent.

Important aspects of the NMHA design are summarized in Table 3.1. Simple equations for R_r, R_l, E_θ, and E_ϕ, which are related to radiation production, have been presented by Kraus [8]. A useful expression for the inductive reactance (X_L) has been developed by Wheeler [9]. However, a correct expression for the capacitive reactance (X_C) has not yet been presented; we plan to develop the appropriate equation for this value. We also compare the theoretical values of the antenna quality factor (Q) with the experimental results. We then consider an important design equation that can be used to determine the self-resonant structures. This equation is derived from the equations for X_L and X_C, and its accuracy is confirmed by comparison of the calculated and simulated results. Using these equations, we can design small antennas with high gain. Because the radiation patterns are almost constant, the antenna efficiency is important for achieving high gain. Finally, the impedance-matching method is important, and three methods are usually considered. However, in the first method among these, the circuit method, the antenna gain is greatly reduced because of the accompanying ohmic resistances of the circuit elements.

Aspect	Features	Comments
Equations of electrical characteristics	Input resistance: R_r, R_l Radiation fields: E_θ, E_ϕ Input reactance: X_L, X_C Q factor	Antenna efficiency Polarization Self-resonance Bandwidth
Self-resonant structure	Determine relation between N, H, D: Using $X_L = X_C$ condition	Design equation must be developed
Design data for high antenna performance	Antenna efficiency	Low ohmic resistance is necessary
Impedance matching	Circuit method Off-center feed Tap feed	Not suitable Limited application Most useful

Table 3.1 Important aspects of NMHA design

To estimate the electrical characteristics of the NMHA, we perform electromagnetic simulations based on the method of moments (MoM) using a commercial simulator, FEKO.

We compare the simulated results with the experimental results. By appropriate choice of the simulation parameters, we can obtain reliable results.

3.2 Equations for main electrical characteristics
3.2.1 Equations of electrical constants for radiation

The radiation characteristics of small antennas are estimated from the antenna input impedance, which is given by

$$Z_{in} = R_{rD} + R_{rL} + R_l + j(X_L - X_C) \tag{3.1}$$

Here, R_{rD} is the radiation resistance of the small dipole; R_{rL}, the radiation resistance of the small loops; and R_l, the ohmic resistance of the antenna wire. X_L and X_C are the inductive and capacitive reactances, respectively. The exact expressions for X_L and X_C will be discussed in the later sections.

We now summarize the expressions for the radiation characteristics.

a. Small dipole [10]

The radiation characteristics of the small dipole are given by the following expressions, in which the structural parameters shown in Fig. 3.1 are used:

$$Rr_D = 20\pi^2 \left(\frac{H}{\lambda} \right)^2 \tag{3.2}$$

Here, λ is the wavelength.

$$E_\theta = \frac{IHe^{-j\kappa R}}{j \, 4\pi\omega\varepsilon} \left(\frac{1}{R^3} + \frac{j\kappa}{R^2} - \frac{\kappa^2}{R} \right) \sin\theta \tag{3.3}$$

Here, I is the antenna current, R is the distance from the antenna, and k is the wave number. The terms $1/R^2$ and $1/R^3$ represent the static electric field and the inductive electric field, respectively. The values of $1/R^2$ and $1/R^3$ decrease rapidly as R increases. The $1/R$ term indicates the far electric field and corresponds to the radiated electric field.

b. Small loop [11]

The radiation characteristics of the small loops are given by the following expressions, in which the structural parameters shown in Fig. 3.1 are used:

$$R_{rL} = 320\pi^6 (a/\lambda)^4 \, n^2 \tag{3.4}$$

Here, a and n indicate the radius of the loop and the number of turns, respectively.

$$E_\phi = \frac{\omega\mu IS e^{-j\kappa R}}{4\pi} \left(-\frac{j}{R^2} + \frac{\kappa}{R} \right) \sin\theta \tag{3.5}$$

The $1/R$ term represents the radiated electric field. Here, I is the loop antenna current, and S is the area of a loop.

3.2.2 Equations for input reactance of NMHA [12]

The equivalent model of the small dipole and small loops (shown in Fig. 3.1) cannot be used for the expressions for X_L and X_C. For the stored electromagnetic power of the NMHA, highly precise electromagnetic models must be developed.

a.   Self-resonant structure

The self-resonant structures of an NMHA are important when designing reactance equations. These structures can be obtained from the structural parameters that satisfy the condition $X_L = X_C$. The aforesaid parameters can be easily identified by electromagnetic simulations, but such simulations are tedious and time-consuming.. An alternative method would involve the use of design equations. However, a convenient equation for determining the resonant structure has not yet been developed; we plan to develop such an equation.

The self-resonant structures calculated from simulations are shown in Fig. 3.2. Here, the 315-MHz data used for the TPMS are shown. For a given N value, a strict relationship between H and D is determined. As N increases, D decreases rapidly, indicating that the total wire length (L_0) of the antenna changes only to a slight extent. The calculated wire lengths are shown in Fig. 3.3. The values of L_0/λ range from 0.35 to 0.72. These data are important for choosing the appropriate wire length when fabricating an actual antenna.61.38
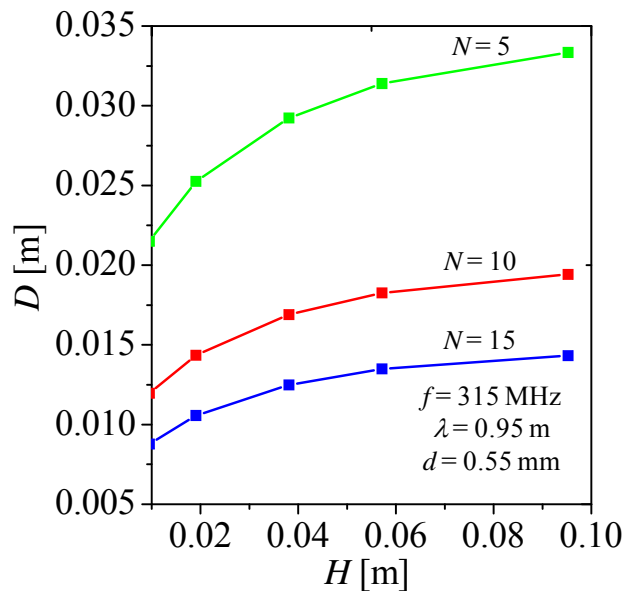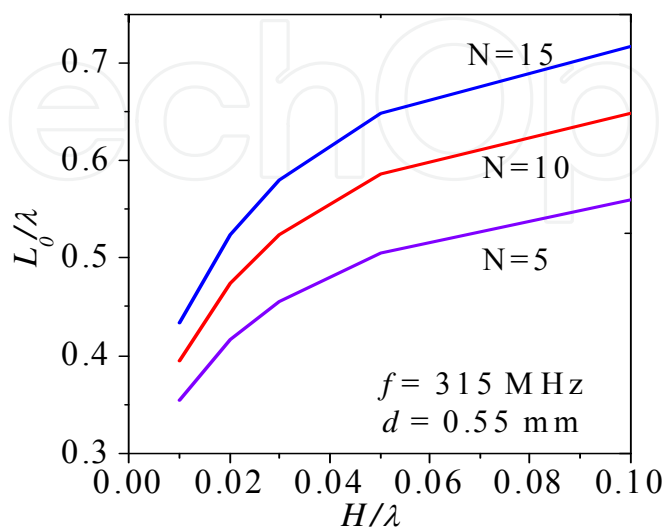
Fig. 3.2 NMHA resonant structures

Fig. 3.3 NMHA wire lengths (L_0)

The typical electrical performance of the self-resonant structure is the excited current in the antenna. The peak electrical currents of the resonance are shown in Fig. 3.4. To illustrate the physical phenomena in detail, sequential N values of 4, 5, and 6 are selected. In the calculation, the feed voltage V is set to 1 V. The current values show a peak near the resonant structures. The current decreases rapidly with an increase in the distance between the resonant structure and the measurement point. The condition $X_L = X_C$ is important for the production of strong radiation currents. Another important point to be noted is that the peak current values are almost inversely proportional to H. Since $V = R_{in}I_M$, an increase in I_M implies a decrease R_{in}. As exepected, R_{in} decreases as H decreases.
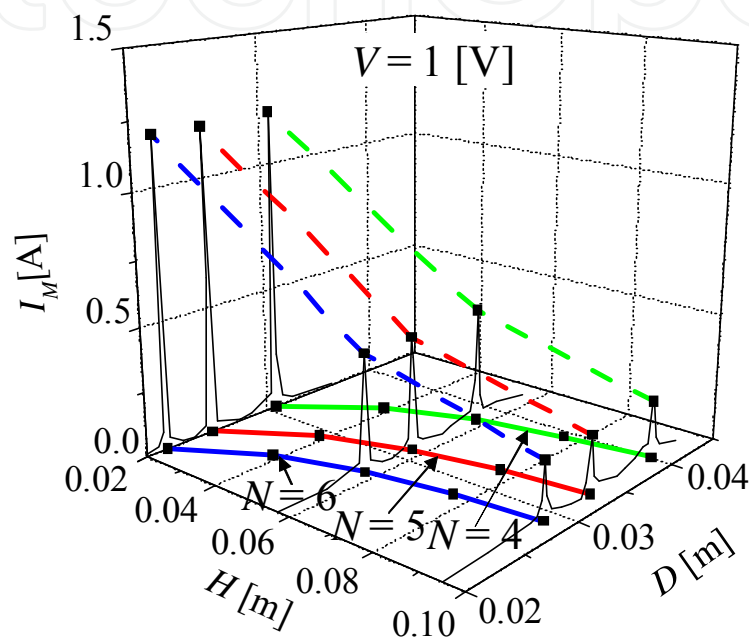
Fig. 3.4 Maximum currents near the resonances

b.   Equation for inductive reactance

The calculated magnetic field distributions are shown in Fig. 3.5. It can be seen that the magnetic field vectors constantly pass through the coil. The field distributions around the anntena are similar to those in the case of a conventional coil. No unique distributions are observed.

The equation for the antenna inductance (L_W) was established by Wheeler [9]. By applying Wheeler's equation to the center-feed antenna, we obtain

$$L_W = \frac{19.7ND^2}{9D + 20H} \times 10^{-6} \quad [\text{H}] \tag{3.6}$$

Here, the unit [H] stands for Henry.
The inductive reactance (X_L) is given by

$$X_L = \omega L_W \quad [\Omega] \tag{3.7}$$

The calculated inductive reactance X_L (Fig. 3.6) is rather large: it ranges from 59 Ω to 205 Ω. In this figure, the dependence of X_L on the structural parameters (N, D, and H) is explained by taking into account Eq. (3.6). The relation between X_L and H is determined on the basis of

the denominator in Eq. (3.6). The change in X_L with N is rather slow and is determined by the term ND^2 in this equation.
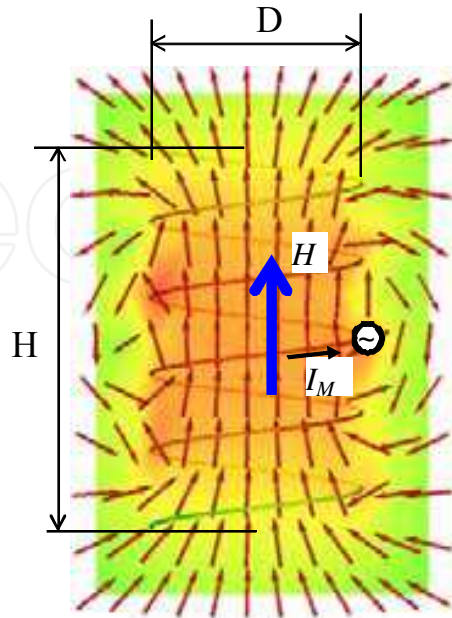

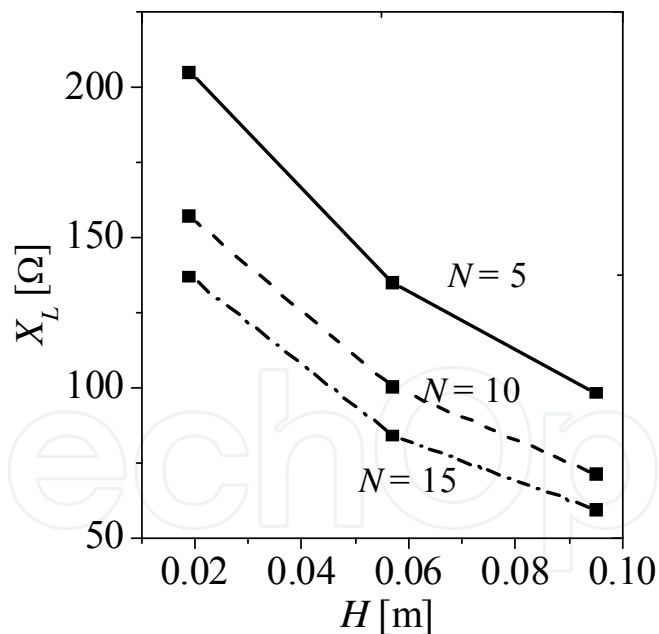Fig. 3.5 Magnetic field distribution

Fig. 3.6 Inductive reactance

c.   Equation for capacitive reactance

In this chapter, we discuss the development of a useful expression for capacitive reactance. The calculated electric field distributions are shown in Fig. 3.7. The directions of the electric field vectors appear to be unique. At the edges of the antenna, the vectors appear to converge or diverge in specific areas. These areas form short cylinders of height αH, as shown by the dashed lines.
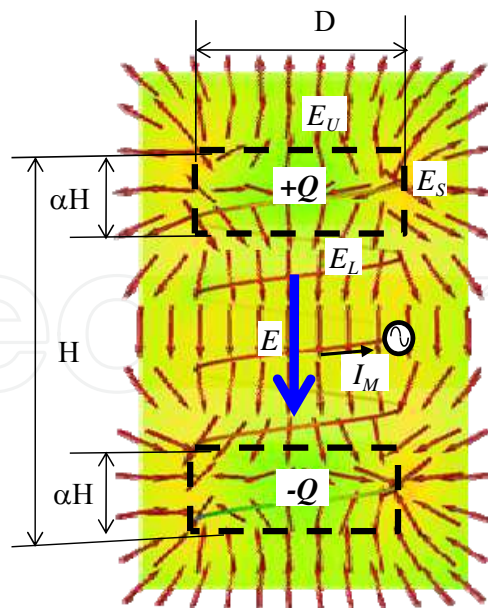
Fig. 3.7 Electric field distributions
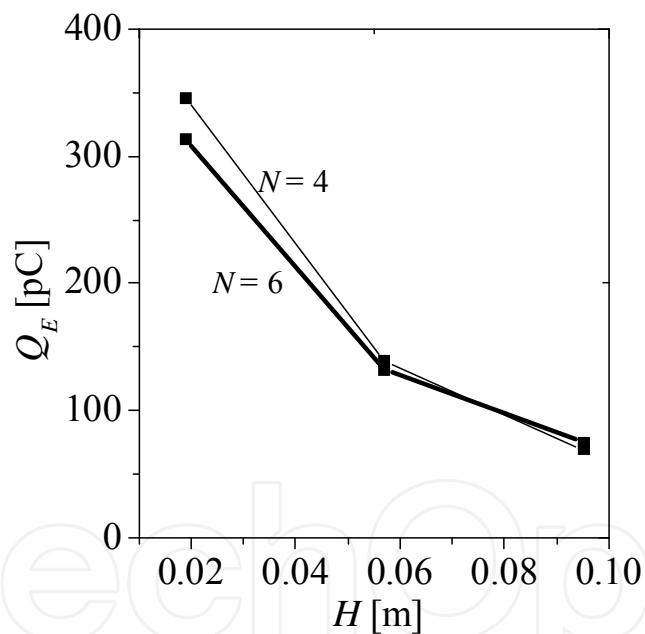
Fig. 3.8 Stored charge

By applying the divergence theorem of Maxwell's equation, we calculate the charge stored in a cylinder from the following equation:

$$Q = \varepsilon \iint E dS = \varepsilon \left\{ \iint E_S dS + \iint E_L dS + \iint E_U dS \right\} \quad [\text{C}] \tag{3.8}$$

Here, the unit [C] stands for Coulomb. Surface integrals over the side wall, lower disc, and upper disc of the cylinder are evaluated.

The calculated Q values are shown in Fig. 3.8. By comparing the cylinder height coefficients (α) of many resonant structures, we estimated the value of α in the present study to be 0.21.

The Q values are inversely proportional to H; this trend agrees well with the relationship between I_M and H shown in Fig. 3.4. This agreement corresponds to the relation $Q = I_M / \omega$. The magnitude of ω (= $2\pi f$) is 2×10^9. If we set I_M and H to 1.2 A and 0.02 m, respectively, in Fig. 3.4, we have

$$I_M / \omega = 1.2 / (2 \times 10^9) = 600 \times 10^{-12} \tag{3.9}$$

The value derived using Eq. (3.9) corresponds well with the Q and H values (400 pC and 0.02 m, respectively) determined from Fig. 3.8. Thus, the use of Eq. (3.8) is justified.

The next step is to derive an expression for the capacitance (C) on the basis of Eq. (3.8). The relationship between Q and C depends on the electric power (We). Two expressions for We are given as follows.

$$W_e = \frac{Q^2}{2C} \tag{3.10}$$

This expression gives the total electric power stored in the +Q and –Q capacitor.

$$W_e = \zeta \iiint \varepsilon E_L^2 dv / 2 \tag{3.11}$$

The volume integral gives the electric power in the NMHA. The coefficient ζ is introduced to express the total power.

By equating Eqs. (3.10) and (3.11), we obtain an expression for C:

$$C = \frac{\left\{\varepsilon \iint E dS\right\}^2}{\zeta \varepsilon \iiint E_L^2 dv} \tag{3.12}$$

Eq. (3.12) can be converted into an expression based on the structural parameters:

$$C = \frac{\varepsilon^2 N \left\{\pi D a H E_S + \pi(\frac{D}{2})^2 (E_U + E_L)\right\}^2}{\zeta \varepsilon E_L^2 \pi(\frac{D}{2})^2 (1 - 2\alpha) H} = \frac{3.82 \varepsilon \pi N (4.4 \alpha H + D)^2}{4\zeta (1 - 2\alpha) H} \tag{3.13}$$

Here, we use the conditions $E_S = 1.1(E_L + E_U)$ and $E_S = 2.15 E_L$, on the basis of the simulation results; α is the cylinder height shown in Fig. 3.7. For the N dependence, we recall the ND^2 term in Eq. (3.6). To model the gradual change of C with N we multiply N by $(4.4aH+D)^2$.

The expression for X_C is obtained from Eq. (3.13):

$$X_C = \frac{1}{\omega C} = \frac{4\zeta (1 - 2\alpha) H}{3.82 \omega \varepsilon \pi N (4.4 \alpha H + D)^2} = \frac{279 \lambda H}{\pi N (0.92 H + D)^2} \tag{3.14}$$

Here, we use $\omega \varepsilon = 1/(60\lambda)$ and $\alpha = 0.21$. Moreover, we set ζ to 7.66 for equating X_C with X_L at $N = 10$; see Fig. 3.6.

The calculated X_C values are shown in Fig. 3.9. At $N = 10$, the $X_C = X_L$ condition is achieved (Figs. 3.9 and 3.6). At $N = 5$ and $N = 15$, X_C and X_L are in good agreement with each other. As a fall, agreement of X_C and X_L are well. Thus, Eq. (3.14) is confirmed to be useful.
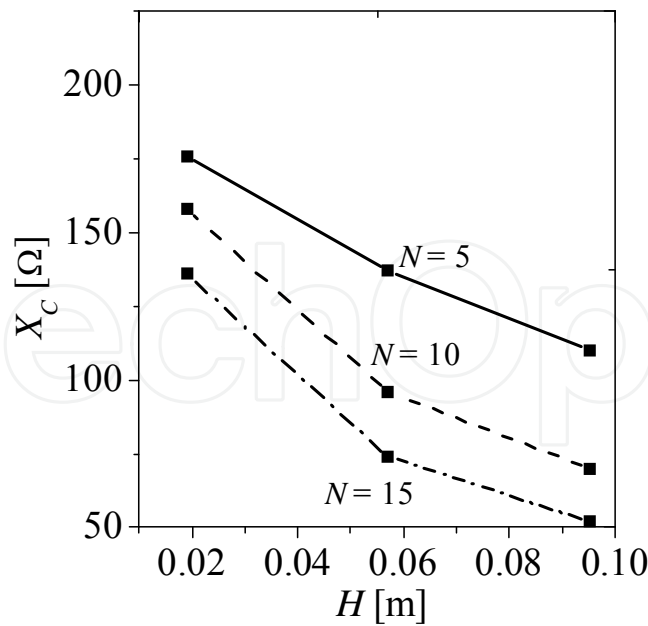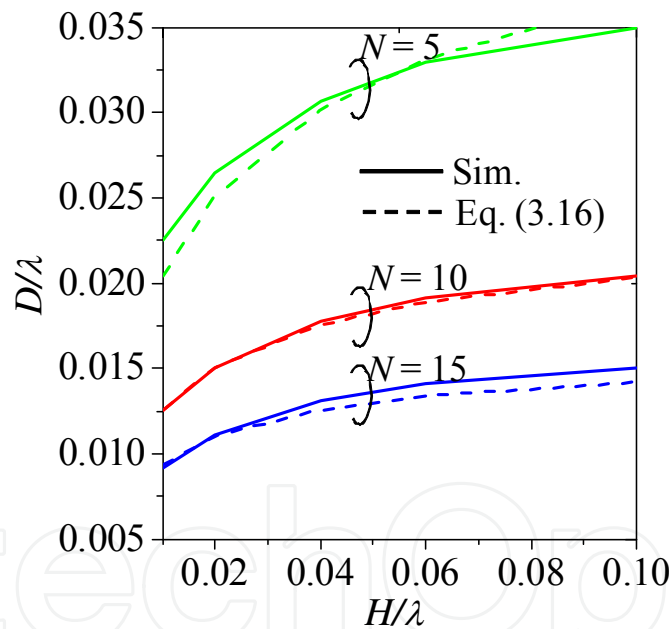
Fig. 3.9 Capacitive reactance

Fig. 3.10 Calculated and simulated self-resonant structures

3.2.3 Design equation for self-resonant structures [12]

The deterministic equation is given by equating Eqs. (3.7) and (3.14). The resulting equation is

$$\omega \frac{19.7ND^2}{9D+20H} \times 10^{-6} = \frac{279\lambda H}{N\pi(0.92H+D)^2} \tag{3.15}$$

To clarify the frequency dependence, we divide the numerator and denominator of Eq. (3.15) by λ^2 and obtain

$$600\pi \frac{19.7N(\frac{D}{\lambda})^2}{9\frac{D}{\lambda} + 20\frac{H}{\lambda}} = \frac{279\frac{H}{\lambda}}{N\pi(0.92\frac{H}{\lambda} + \frac{D}{\lambda})^2} \tag{3.16}$$

An important feature of this design equation is that it becomes frequency-independent when the structural parameters are normalized by the wavelength.

To ensure the accuracy of this equation, the calculated results are compared with the curves in Fig. 3.2. Figure 3.10 shows this comparison. At $N = 10$, curve obtained on the basis of Eq. (3.16) agrees well with that obtained on the basis of the simulation results. At $N = 5$ and $N = 15$, small differences are observed between the two curves; however, the maximum difference is less than 9.4%. Thus, Eq. (3.16) is confirmed to be useful.

3.2.4 Ohmic resistance
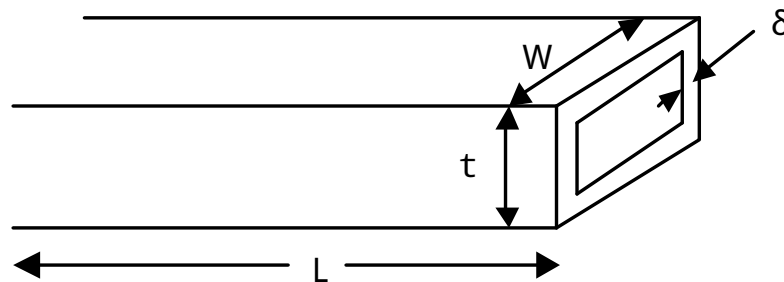
Fig. 3.11 Cross-sectional view of antenna wire

Figure 3.11 shows a cross-sectional view of the antenna wire. The parameters W, t, and L represent the width, thickness, and total length of the wire, respectively, and δ is the skin depth:

$$\delta = \sqrt{\frac{2}{\omega\mu\sigma}} \tag{3.17}$$

Here, σ is the conductance of the wire metal.

If the current is concentrated within the skin depth δ, the ohmic resistance is

$$R_l = \alpha \frac{L}{2(t+W)\delta} \cdot \frac{1}{\sigma} = \alpha \frac{L}{d\delta\pi} \cdot \frac{1}{\sigma} \tag{3.18}$$

Here, α is the coefficient of the tapered current distribution, and d is the wire diameter.

By applying Eq. (3.17) to Eq. (3.18), we obtain the following expression for the ohmic resistance:

$$R_l = \alpha \frac{L}{2(t+W)}\sqrt{\frac{240\pi^2}{2\lambda\sigma}} = \alpha \frac{L\pi}{(t+W)}\sqrt{\frac{30}{\lambda\sigma}} = \alpha \frac{L}{d}\sqrt{\frac{120}{\lambda\sigma}} \tag{3.19}$$

In small NMHAs, because the current distribution becomes sinusoidal, Eq. (3.19) agrees well with the simulation result at $\alpha = 0.6$.

The δ values are shown in Fig. 3.12. Here, a copper wire is considered, and the σ value is set to 5.8×10^7 [1/Ωm]. The t value should be more than four times the δ value. The calculated results, i.e., the results obtained using Eq. (3.19), are shown in Fig. 3.13; an important point to be noted is that the values of R_l are not sufficiently small. By substituting the L_0 value determined from Fig. 3.3 in Eq. (3.19), we can calculate the R_l values for NMHAs. In Fig. 3.3, L_0 is about 0.48 m (0.95×0.5) at 315 MHz, and hence, R_l is approximately 0.7 Ω. If the frequency changes and L and d are changed analogously, R_l becomes inversely proportional to $\sqrt{\lambda}$. The most effective way to reduce R_l is to increase W or d.
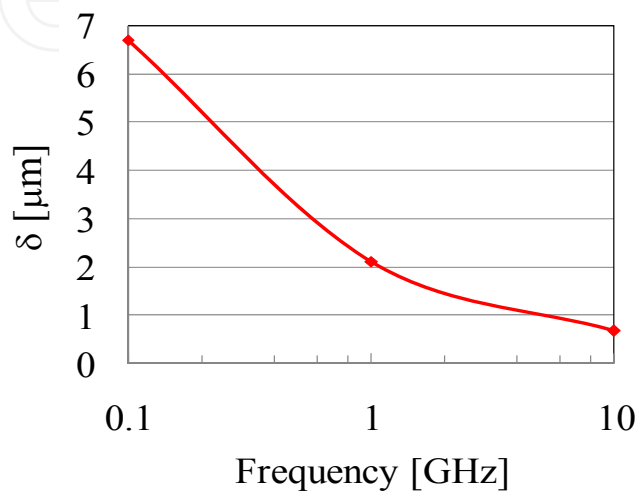
Fig. 3.12 Skin depth (δ)
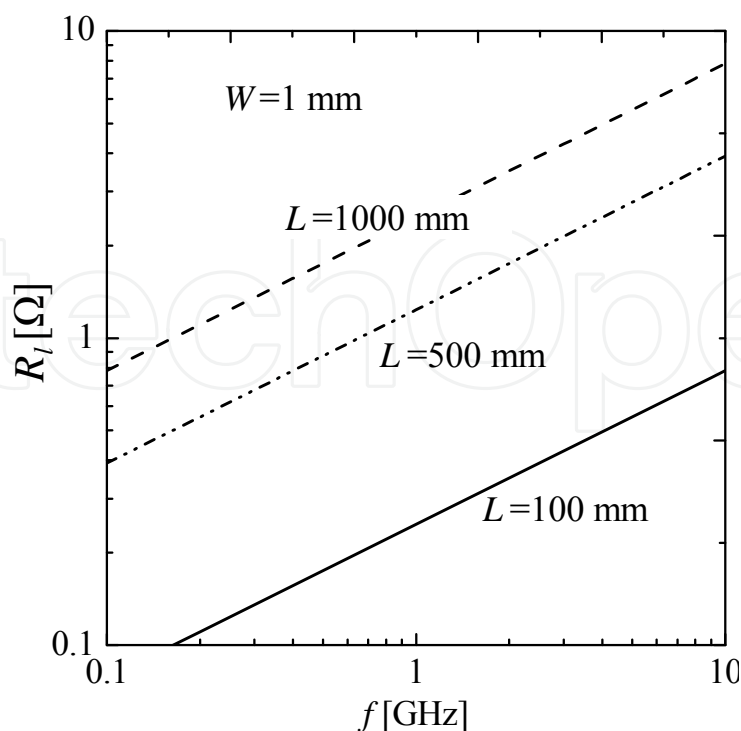
Fig. 3.13 Ohmic resistance

3.2.5 Input resistances

The simulated input resistances (R_{in}) of the self-resonant structures are shown in Fig. 3.14. Here, R_{in} is expressed as follows:

$$R_{in} = R_r + R_l = R_{rD} + R_{rL} + R_l \tag{3.20}$$

For an R_l value of approximately 0.7 Ω, R_l.shares the dominant part of R_{in} at $H = 0.02$ m in Fig. 3.14 In these small antennas, most of the input power is dissipated as ohmic resistance, and only a small component of the input power is used for radiation.
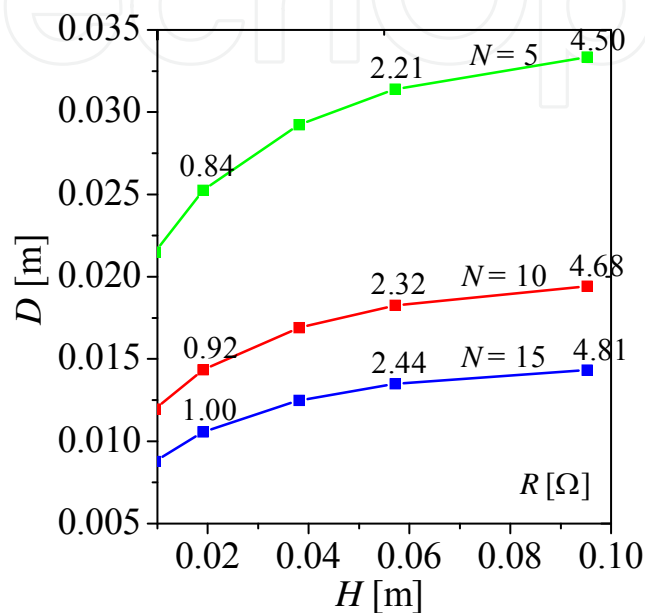

Fig. 3.14 Input resistances

Table 3.2 gives the details of the input resistances. The calculated results, i.e., the results obtained using Eqs. (3.2), (3.4), and (3.17), are compared with the simulated results. The $R_{rD}+R_{rL}$ values determined from the aforementioned equations agree well with the simulated results. The calculated and simulated R_l values also agree well with each other; in the equation, an α value of 0.6 is used. Finally, the R_{in} values are compared, and the antenna efficiencies ($\eta = (R_{rD}+R_{rL})/R_{in}$) are obtained. The calculated and simulated results agree well, and thus, the equations are confirmed to be accurate. Moreover, R_l has a large negative effect on the antenna efficiency.

Structure		$R_{rD}[\Omega]$	$R_{rL}[\Omega]$	$R_l[\Omega]$	$R_{in}[\Omega]$	η[dB]
$N = 5$ $H = 0.02\lambda$	Eq.	0.0790	0.2378	0.6380	0.9548	-4.7911
	Sim.	0.2537		0.5862	0.8399	-5.1988
$N = 15$ $H = 0.02\lambda$	Eq.	0.0790	0.0656	0.8008	0.9453	-8.1554
	Sim.	0.1987		0.7988	0.9975	-7.0067

Table 3.2 Resistances determined by calculation and simulation

3.2.6 Q factor

The Q factor is important for estimating the antenna bandwidth. The radiation Q factor (Q_R) for electrically small antennas is defined as

$$Q_R = \text{stored energy } (E_{sto})/\text{radiating energy } (E_{dis}) \tag{3.21}$$

For antennas, these energies are expressed by the input impedance:

$$E_{sto} = X I^2 \tag{3.22}$$

$$E_{dis} = R_r \tag{3.23}$$

Therefore, Q_{imp} can be expressed as follows:

$$Q_{imp} = X/R_r \tag{3.24}$$

Another expression for the Q factor is based on the frequency characteristics; in this case, the Q factor is referred to as Q_A:

$$Q_A = f_c/\Delta f \tag{3.25}$$

Here, f_c is the center frequency and Δf is the bandwidth. In this expression, a small Q_A value indicates a large bandwidth.

McLean [13] gave the lower bound for the Q factor (Q_M):

$$Q_M = \frac{1}{ka} + \frac{1}{(ka)^3} \tag{3.26}$$

Figure 3.15 shows examples of Q_A and Q_M for NMHAs; Ds is the diameter of the sphere enclosing an NMHA. The antenna structures labeled A and B are those shown in Fig. 3.16. The Q_A values of A and B are based on the measured voltage standing wave ratio (VSWR) characteristics shown in Fig. 3.19. We can see that Q_A is smaller than Q_M, because of the ohmic resistance of the antenna.
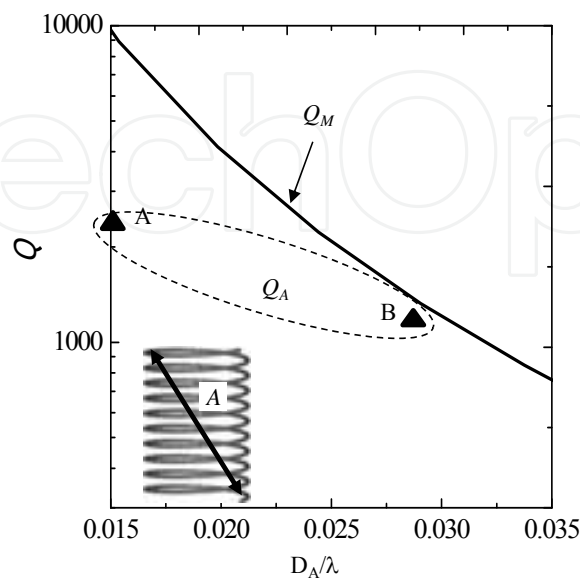

Fig. 3.15 Q factors for NMHA

3.3 Achieving a high antenna gain

The efficiency (η) of a small antenna is defined as

$$\eta = (R_{rD} + R_{rL})/(R_{rD} + R_{rL} + R_l) \tag{3.27}$$

Since (see Table 3.2) R_l is greater than R_r (=R_{rD} + R_{rL}), R_l must be decreased in order to achieve high antenna efficiency. From Eq. (3.19), it is clear that increasing the antenna wire width (W) or diameter (d) is the most effective way to reduce R_l. If W is increased, it would be necessary to ensure that neighboring wires are well separated from each other.

By substituting Eqs. (3.2), (3.4), and (3.19) in Eq. (3.27), we can calculate η; the result is shown in Fig. 3.16.

It can be seen that η decreases with a decrease in H and D. In this case, we use a very narrow antenna wire (d = 0.05 mm). At points A and B, η is 10% (-10 dB) and 25% (-6 dB), respectively. The relationship between the antenna gain (G_A) and η is given by

$$G_A = G_D \, \eta \qquad \text{[dBi]} \tag{3.28}$$

Here, G_D is the directional gain of the antenna. In electrically small antennas, G_D remains almost constant at 1.8 dBi. The antenna gains at points B and A are G_A = -4.2 dBi and -8.2 dBi, respectively. Given the small antenna size, these gains are large. Moreover, the gains can be increased if a thicker wire is used. In conclusion, it is possible to achieve a high gain when using small antennas.
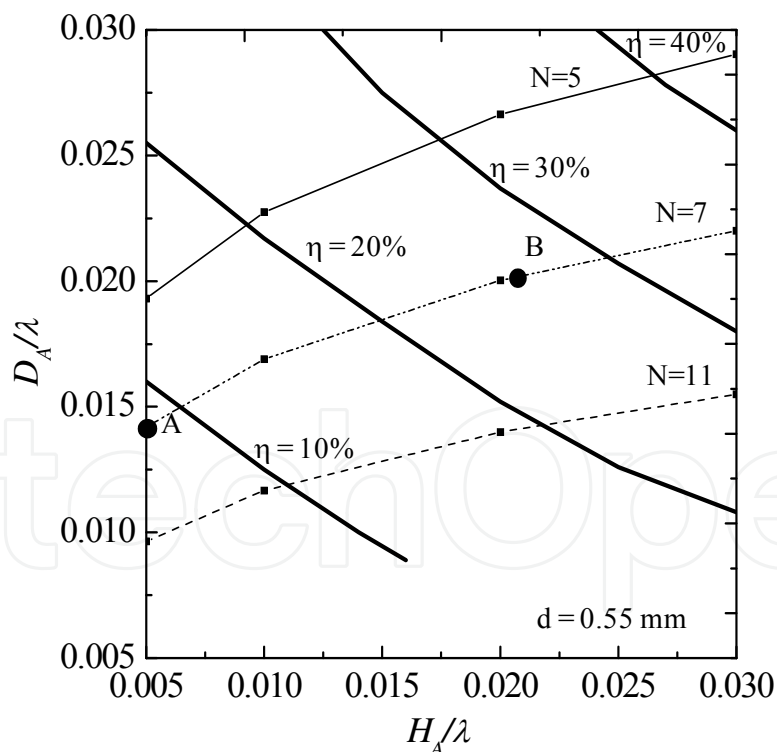

Fig. 3.16 Efficiency of NMHA

3.4 Examples of electrical performance

In order to investigate the realistic characteristics, we fabricated a 0.02λ antenna (point B in Fig. 3.16), as shown in Fig. 3.17. The antenna impedances are measured with and without a

tap feed. The tap structure is designed according to the procedure given in Section 4.2.4. Excitation is achieved with the help of a coaxial cable. The coaxial cable is covered with a Sperrtopf balun to suppress the leak current. The measured and calculated impedances are shown in Fig. 3.18. The results agree well both with and without the tap feed, thereby confirming that the measurement method is accurate. The tap feed helps in bringing about an effective increase in the antenna input resistance. The bandwidth characteristics are shown in Fig. 3.19; the measured and simulated results agree well. The bandwidth at VSWR < 2 is estimated to be 0.095%.
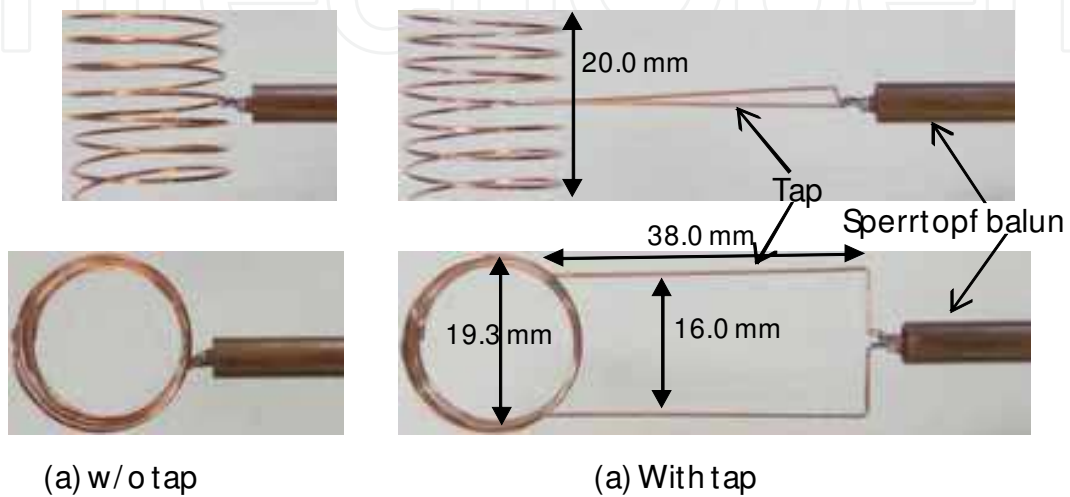
Fig. 3.17 Fabricated antenna ($H = 0.021\lambda$, $D = 0.020\lambda$)
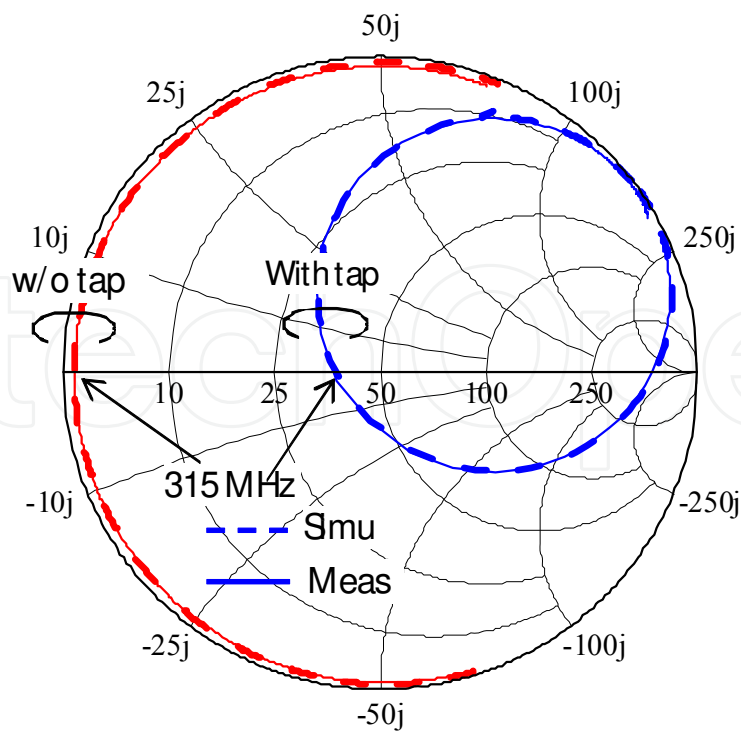
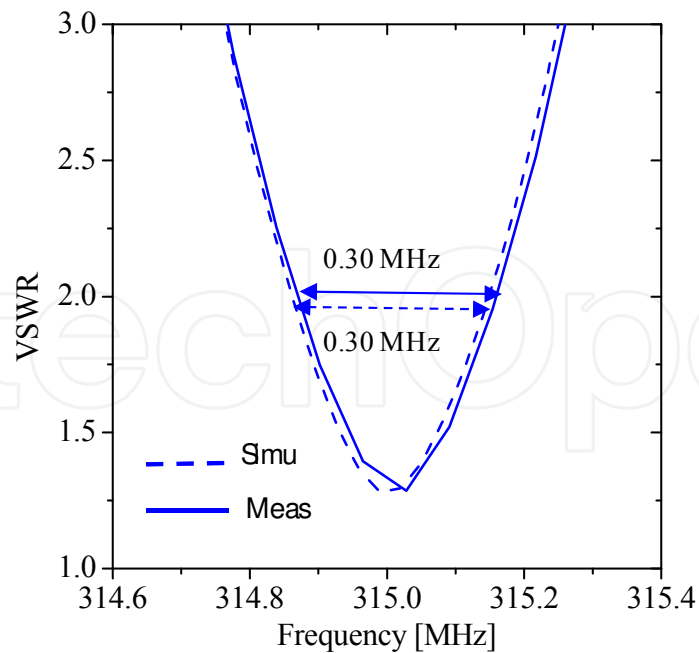Fig. 3.18 Antenna input impedance

Fig. 3.19 VSWR characteristics

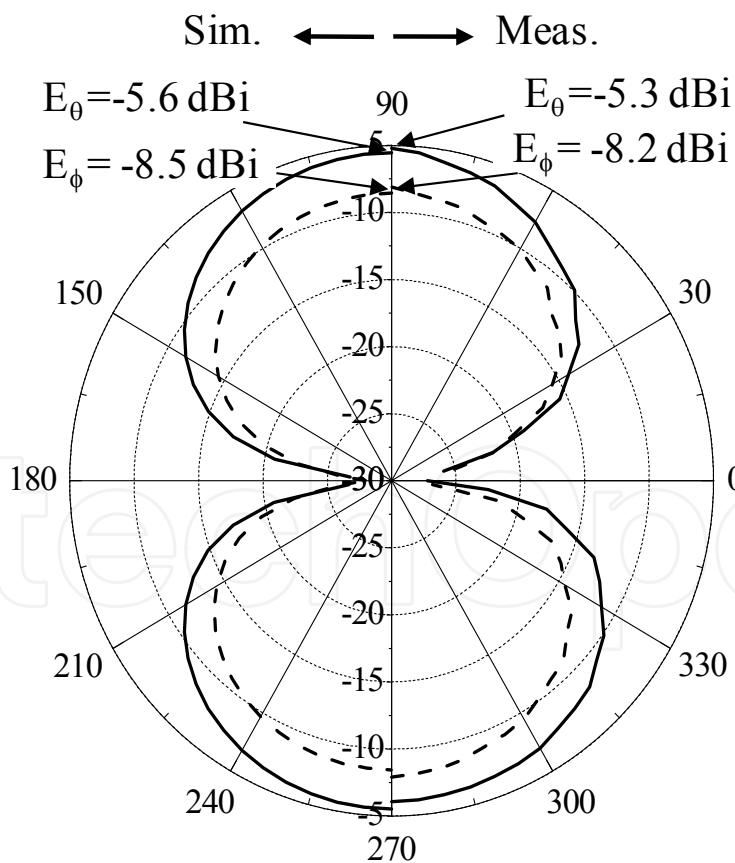

Fig. 3.20 Radiation patterns

As can be seen from Fig. 3.20, the measured and simulated radiation characteristics are in good agreement. The E_θ component corresponds to the radiation from the electric current

source shown in Fig. 3.1, and the E_ϕ component corresponds to the radiation from the magnetic current source shown in Fig. 3.1. There is a 90° phase difference between the E_θ and E_ϕ components. Therefore, the radiated electric field is elliptically polarized. Because the magnitude difference between the E_θ and E_ϕ components is only 3 dB, the radiation field is approximately circularly polarized. The magnitude of the E_θ and E_ϕ components correspond to R_{rD} in Eq. (3.2) and R_{rL} in Eq. (3.4). The antenna gains of the E_θ and E_ϕ components can be estimated by the η value shown in Fig. 3.16. The value $\eta \times G_D$ (G_D indicates the directional gain of 1.5) of structure B becomes -4 dBi. This value agrees well with the total power of the E_θ and E_ϕ components.

4. NMHA impedance-matching methods

4.1 Comparison of impedance-matching methods

For the self-resonant structures of very small NMHAs, effective impedance-matching methods are necessary because the input resistances are small. There are three well-known impedance-matching methods: the circuit method, the displaced feed method, and the tap feed method as shown in Fig. 4.1. In the circuit method, an additional electrical circuit composed of capacitive and inductive circuit elements is used. In the displaced feed method, an off-center feed is used. The amplitude of the resonant current (I_{dis}) is lower at the off-center point than at the center point (I_M), and hence, the input impedance given by $Z_{in} = V/I_{dis}$ is increased. As the feed point approaches the end of the antenna, the input resistance approaches infinity. This method is useful only for objects with pure resistance. Since the RFID chip impedance has a reactance component, this method is not applicable to RFID systems. In the tap feed method, an additional wire structure is used. By appropriate choice of the width and length of the wire, we can achieve the desired step-up ratio for the input resistance. Moreover, the loop configuration can help produce an inductance component, and therefore, conjugate matching for the RFID chip is possible. This feed is applicable to various impedance objects.

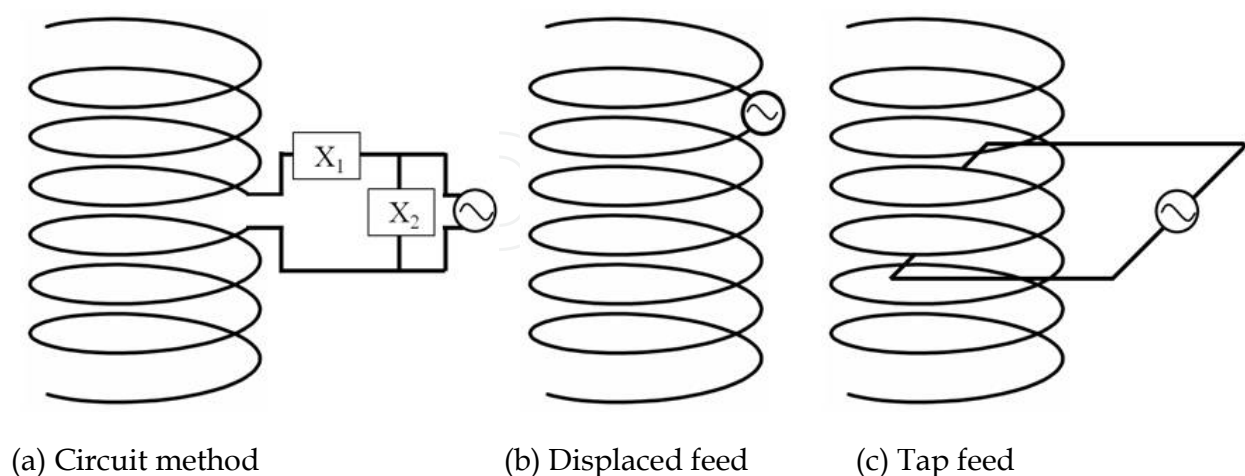(a) Circuit method   (b) Displaced feed   (c) Tap feed

Fig. 4.1 Configurations of impedance matching methods

The features of the three methods are summarized in Table 4.1. For the circuit method, the capacitive and inductive elements are commercialized as small circuit units. These units have appreciable ohmic resistances.

If the NMHA input resistances are around 1 Ω, the ohmic resistance values become significant. This method is not suitable for small antennas with small input resistances. For the displaced feed method, the matching object must have pure resistance. The tap feed method can be applied to any impedance object, but it is not clear how the tap parameters can be determined when using this method.

Method	Advantages	Disadvantages	Design
Circuit method [8]	With capacitance and inductance chips, matching is easily achieved	Severe reduction in antenna gain by chip losses	Theoretical method has been established
Displaced feed [9]	Simple method of shifting a feed point No reduction in antenna gain	Limited to pure resistance objects	Displacement position is easily found empirically
Tap feed [10]	Uses additional structure No reduction in antenna gain Applicable to any object	Additional structure increases antenna volume	Design method has not been established

Table 4.1 Comparison of impedance-matching methods

4.2 Design of tap feed structure [14]
4.2.1 Derivation of equation for input impedance
The tap feed method has been used for the impedance matching of a small loop antenna [15]. The tap is designed using the equivalent electric circuit. The tap configuration for the NMHA is shown in Fig. 4.2. The antenna parameters D and H are selected such that self-resonance occurs at 315 MHz. The tap is attached across the center of the NMHA, and the tap width and tap length are denoted as a and b, respectively. The equivalent electric circuit is shown in Fig. 4.3. Here, L, C, and R are the inductance, capacitance, and input resistance, respectively. The tap is excited by the application of a voltage V; M_A is the mutual inductance between the NMHA and the tap.

In the network circuit shown in Fig. 4.3, the circuit equations for the NMHA and the tap are as follows:

$$\left\{\frac{1}{j\omega C}+R+j\omega(L-M_A)\right\}I_A+j\omega M_A(I_A-I_T)=0 \tag{4.1}$$

$$j\omega(L_T-M_A)I_T+j\omega M_A(I_T-I_A)=V \tag{4.2}$$

From the above equations, the input impedance ($Z_{in} = V/I_T$) of the NMHA can be deduced:

$$Z_{in} = \frac{R(\omega M_A)^2}{R^2 + (\omega L - \frac{1}{\omega C})^2} + j \frac{R^2(\omega L_T) - (\omega M_A)^2(\omega L - \frac{1}{\omega C}) + \omega L_T(\omega L - \frac{1}{\omega C})^2}{R^2 + (\omega L - \frac{1}{\omega C})^2} \qquad (4.3)$$

Here, the tap inductance (L_T) is given by [16]:

$$L_T = \frac{\mu}{\pi}\left[b\ln(\frac{4ab}{d(b + \sqrt{a^2 + b^2})}) + a\ln(\frac{4ab}{d(a + \sqrt{a^2 + b^2})}) + 2(d/2 + \sqrt{a^2 + b^2} - b - a) \right] \qquad (4.4)$$
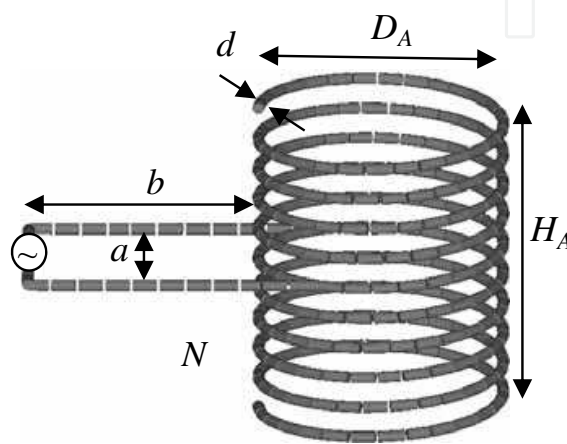

Fig. 4.2 Tap configuration for NMHA
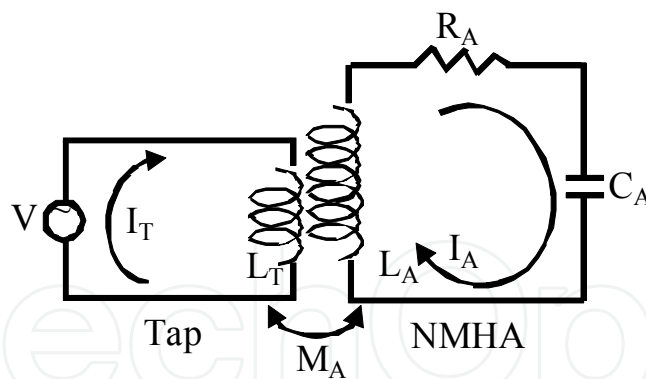
Fig. 4.3 Equivalent circuit for tap feed

4.2.2 Simple equation for step-up ratio

At the self-resonant frequency ($\omega_r = 2\pi f_r$), the imaginary part of Eq. (4.3) becomes zero. Therefore, we have

$$R^2(\omega_r L_T) - (\omega_r M_A)^2(\omega_r L - \frac{1}{\omega_r C}) + (\omega_r L - \frac{1}{\omega_r C})^2 = 0 \qquad (4.5)$$

If the variable of the above equation is replaced by ($\omega_r L - 1/\omega_r C$) = α, this expression becomes second-order in α. The two solutions are

$$\alpha(\pm) = \frac{\omega_r M_A^2 \pm \sqrt{\omega_r^2 M_A^4 - 4R^2 L_T^2}}{2L_T} \tag{4.6}$$

We label these two solutions $\alpha(+)$ and $\alpha(-)$. For these α values, the resonant points are shown in Fig. 4.4.
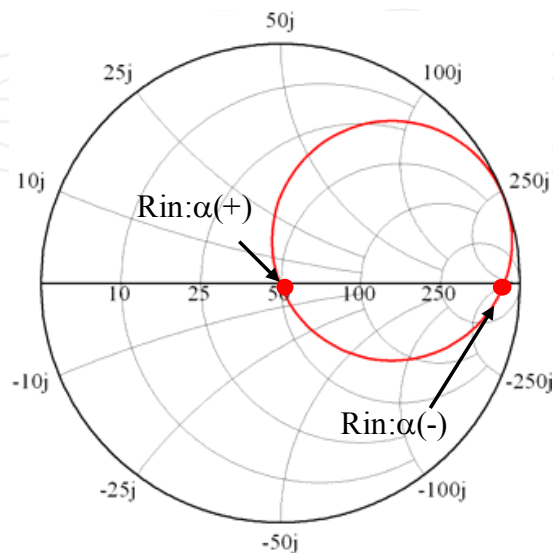

Fig. 4.4 Resonant points

In the root of Eq. (4.6), the following assumption is applicable. This assumption is valid when the tap width (*a*) is nearly equal to the antenna diameter (*D*):

$$\omega_r^2 M_A^4 \rangle\rangle 4R^2 L_T^2 \tag{4.7}$$

Then, the expression for α becomes simple:

$$\alpha(+) = \frac{\omega_r M_A^2}{L_T} \tag{4.8}$$

By using $\alpha(+)$ in Eq. (4.3), we can derive an expression for the input resistance (R_{in}):

$$R_{in} = R(L_T / M_A)^2 \tag{4.9}$$

Finally, the step-up ratio (γ) of the input resistance can be simply expressed as

$$\gamma = \left(L_T / M_A\right)^2 \tag{4.10}$$

The important point to be noted in this equation is that M_A has a strong effect on the step-up ratio. In the following section, the calculation method and M_A results are presented.

4.2.3 Calculation method and results for mutual inductance

The calculation structure is shown in Fig. 4.5. B_A is the magnetic flux density in the NMHA, and I_T is the tap current.
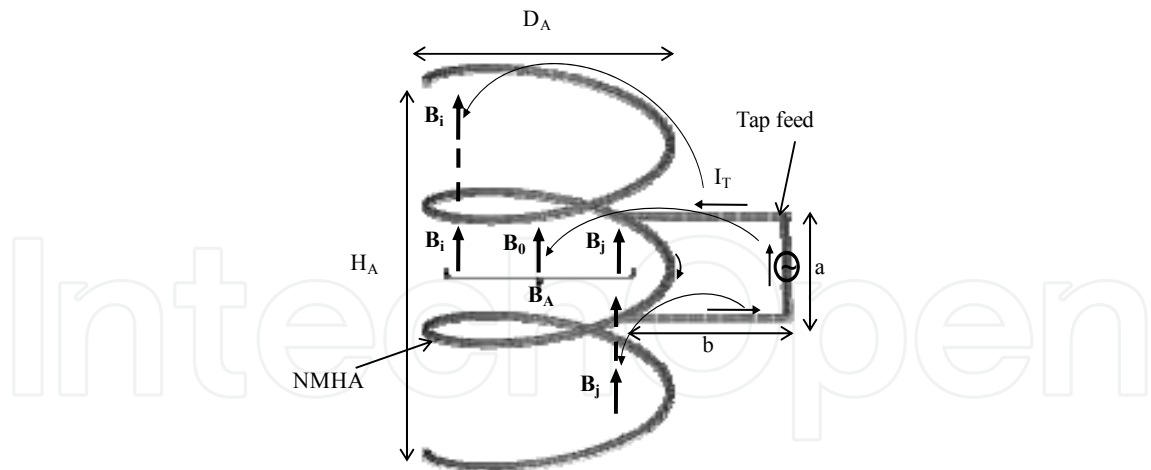M_A can be calculated using the following equation [17]:

Fig. 4.5 Calculation structure

$$M_A = \frac{\int_S \mathbf{B}_A \cdot d\mathbf{S}}{I_T} = \frac{\mu \int_S \mathbf{H}_A \cdot d\mathbf{S}}{I_T} \qquad (4.11)$$

Here, B_A is the sum of the B_i values of each loop in Fig. 4.5. The magnetic field (H_i) in each loop is given by

$$H_{0i} = \int_l \frac{I_T}{4\pi r^2} \sin\theta \, dl \qquad (4.12)$$

Here, r represents the distance between a point on the tap and a point inside a loop. In this calculation, a current I_T exists at the center of the tap wire. Therefore, even if the the magnetic field is applied at point close to the tap wire.
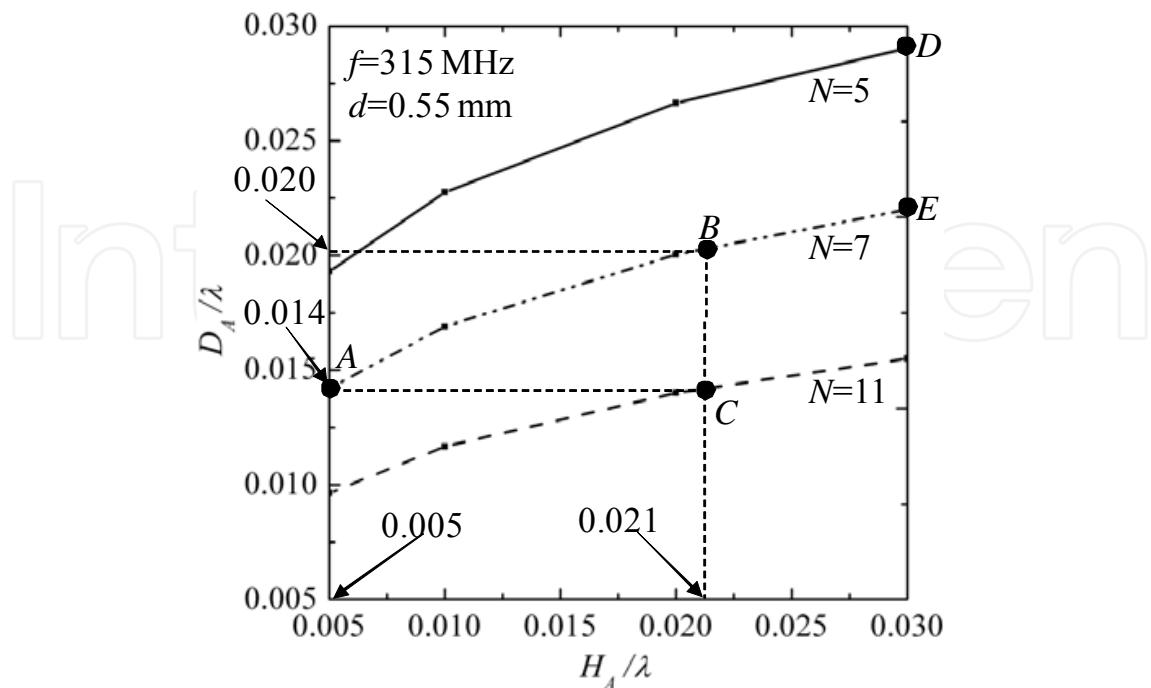
Fig. 4.6 Study structures of NMHA

To establish the design of the tap feed, the L_T/M_A values in Eq. (4.10) must be represented by the structural parameters. Calculations are performed for the structures shown in Fig. 4.6. Points A, B, and C are used to investigate the dependence of M_A on the structural parameters.
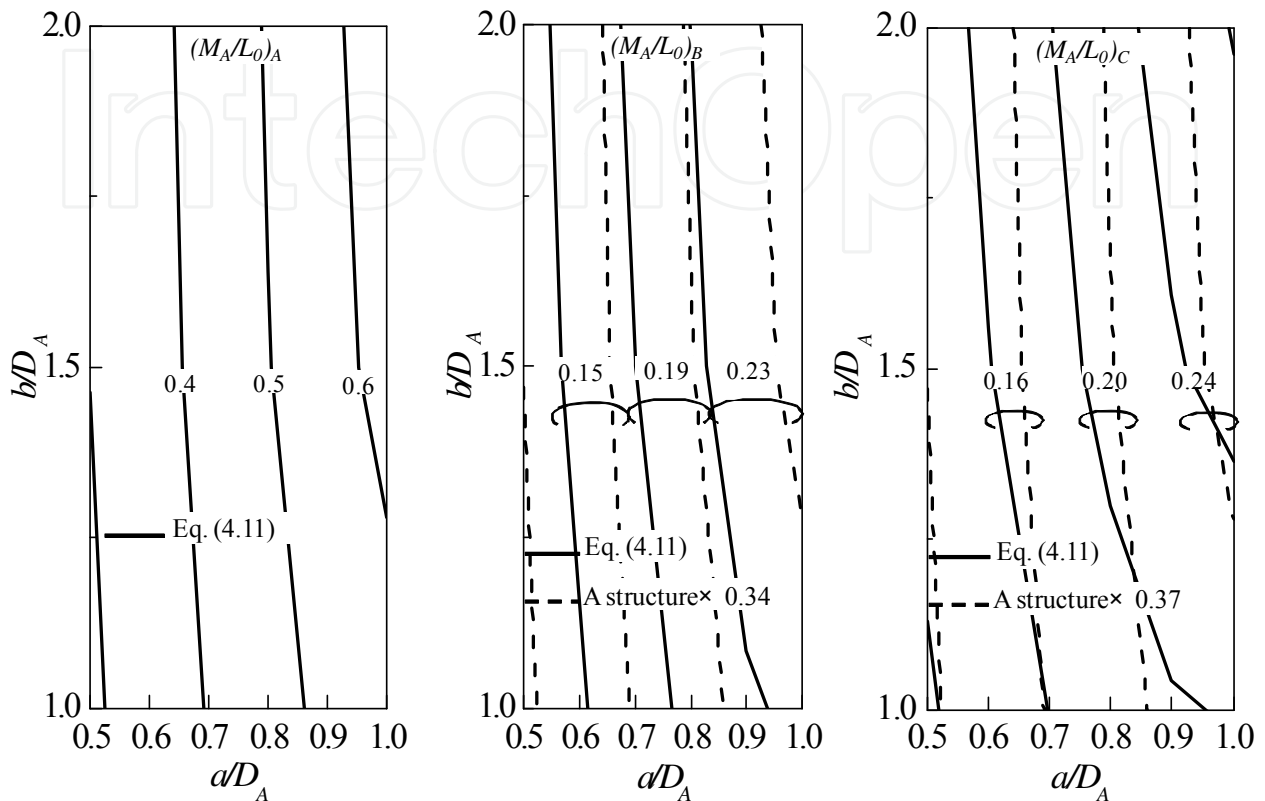
Fig. 4.7 Calculated results: M_A/L_0

The calculated M_A values are shown in Figs. 4.7(a), (b), and (c). The M_A value is normalized by the L_0 value, which is the self-inductance of a small loop with diameter D. L_0 is given by [18]

$$L_0 = \frac{\mu D}{2}\left\{\ln(\frac{8D}{d}) - 1.75\right\} \qquad (4.13)$$

Structure A in Fig. 4.7(a) is used as a reference to determine the dependence of M_A on the structural parameters. Comparison of structures A and B reveals the dependence of M_A/L_0 on H_A and D_A. Taking into account Eq. (4.11), we show that M_A is proportional to D_A/H_A. The D_A/H_A value for structure B becomes 0.34 times that for structure A. In Fig. 4.7(b), the solid lines indicate the calculated results obtained using Eq. (4.11). The dotted lines indicate the transformed values, i.e., the product of the values in Fig. 4.7(a) and 0.34. The data corresponding to the solid and dotted lines are in good agreement, thus confirming that the M_A/L_0 values are proportional to the D_A/H_A value. We now compare structures A and C. Eq. (4.11) shows that M_A is proportional to N/H_A. The N/H_A value for structure C is 0.37 times that for structure A. In Fig. 4.7(c), the solid lines indicate the calculated results obtained using Eq. (4.11). The dotted lines indicate the transformed values, i.e., the product of the values shown in Fig. 4.7(a) and 0.37. The solid and dotted lines agree well, confirming the proportional relationship between M_A/L_0 and N/H_A value. We thus have

$$\frac{M_A}{L_0} \propto \frac{D_A N}{H_A} \qquad (4.14)$$

4.2.4 Universal expression for M_A

The design equation becomes universal if the M_A/L_0 value is expressed in terms of M_0/L_0. Here, M_0 is the mutual inductance between the one-turn loop and a tap. If we introduce a coefficient α_A, M_A/L_0 can be given by

$$\frac{M_A}{L_0} = \alpha_A \frac{D_A N}{H_A} \frac{M_0}{L_0} \qquad (4.15)$$

The M_0/L_0 values calculated using from Eq. (4.11) (assuming $N = 1$) are shown in Fig. 4.8. The M_0/L_0 values show small deviations with the D_A values. If all the structural deviations depending on D_A, H_A, and N are contained in the coefficient term, α_A can be expressed as follows:

$$\alpha = 0.05 + 0.0075N + 4.5\left(\frac{H}{N^2 D}\right) \qquad (4.16)$$

We use $D_A = 0.020\lambda$ (see Fig. 4.8) for the M_0/L_0 values.
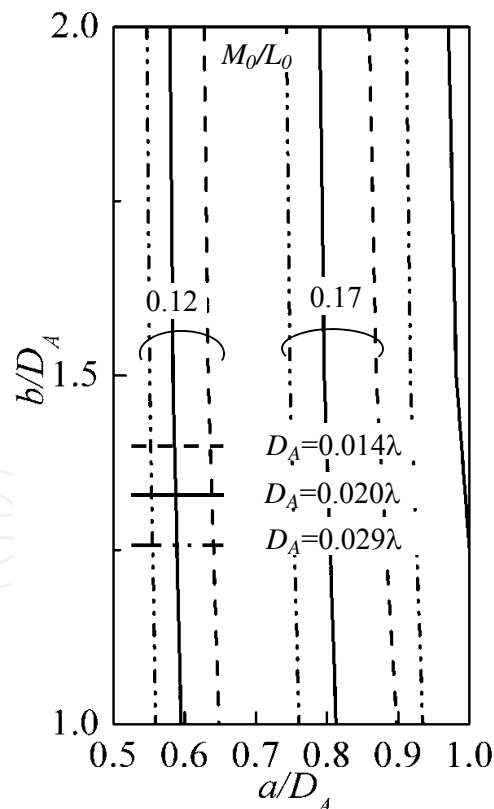
Fig. 4.8 Calculated results: M_0/L_0

4.2.5 Design equation for step-up ratio in NMHA tap feed

By applying Eq. (4.15) to Eq. (4.10), we can express the step-up ratio (γ) as follows:

$$\gamma = (\frac{L_T}{M_A})^2 = (\frac{H_A}{\alpha_A D_A N})^2 (\frac{L_T}{M_0})^2 = (\frac{H_A}{\alpha_A D_A N})^2 \gamma_0 \tag{4.17}$$

This equation is the objective design equation for a tap feed. Here, γ_0 is given by

$$\gamma_0 = (\frac{L_T}{M_0})^2 \tag{4.18}$$

The calculated γ_0 values are shown in Fig. 4.9. For each γ_0, the tap structural parameters a/D_A and b/D_A are given.
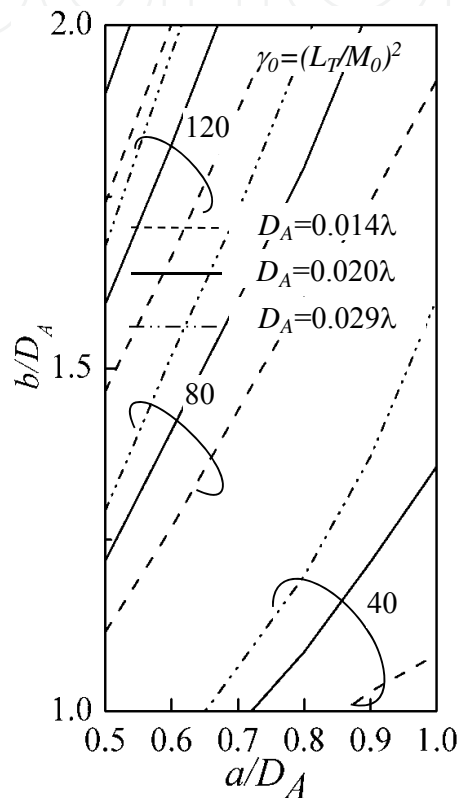

Fig. 4.9 Calculated results: γ_0

4.2.6 Design procedure for tap feed

We now summarize the design procedure. First, the self-resonant NMHA structure is determined on the basis of Fig. 3.2 or Eq. (3.16). Then, the antenna input resistance is estimated using Eqs. (3.2), (3.4), and (3.19). The requested γ value is determined by taking into account the feeder line impedance. Then, Eq. (4.17) is used to determine the tap structure. The γ_0 value is determined by substituting the antenna parameters and γ value in Eq. (4.17). The final step involves the use of the data provided in Fig. 4.9. The objective γ_0 curve in Fig. 4.9 is identified Then, the relation between a/D_A and b/D_A is elucidated, and a suitable combination of a/D_A and b/D_A is selected.

5. Antenna design for RFID tag

In this section, the proximity effect of a metal plate on the self-resonant structures and radiation characteristics of the antenna is clarified through simulation and measurement. An

operating frequency of 953 MHz is selected, and antenna sizes of 0.03λ–0.05λ are considered. We discuss the fabrication of tag antennas for Mighty Card Corporation [19].

5.1 Design of low-profile NMHA [20]

The projection length of the NMHA is reduced by adopting a rectangular cross section, so that the antenna can be used in an RFID tag. The simulation configuration is shown in Fig. 5.1. The antenna thickness is T, and the size of the metal plate is M. The spacing between the antenna and the metal plate is S. The equivalent electric and magnetic currents are I and J, respectively. E_θ and E_ϕ correspond to the radiation from the electric and magnetic currents, respectively.
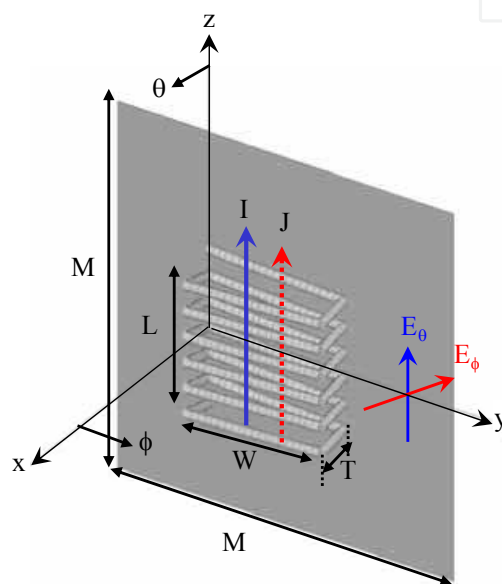
Fig. 5.1 Simulation configuration

The most important aspect of the antenna design is the self-resonant structure. The self-resonant structure without a metal plate is shown in Fig. 3.10. The design equation (Eq. (3.16)) is not effective when a metal plate is present in the vicinity of the antenna. Therefore, the self-resonant structure is determined by electromagnetic simulations. The calculated self-resonant structures are shown in Fig. 5.2; T and N are variable parameters. Other parameters, such as d, S, and M are shown in the figure. For small values of T, large W values are required so that the cross-sectional area is maintained at a given value. For smaller values of N, too, large W values are required so that the individual inductances of the cross-sectional areas are increased.

An example of the input impedance in the structure indicated by the triangular mark at $T = 3$ mm is shown in Fig. 5.3. At 953 MHz, the input impedance becomes a pure resistance of 0.49 Ω. Because the antenna has a small length of 0.04λ, the input resistance is small. The radiation characteristics are shown in Fig. 5.4. To simplify the estimation of the radiation level, the input impedance mismatch is ignored by assuming a "no mismatch" condition in the simulator. The dominant radiation component is E_ϕ, which corresponds to the magnetic current source. Surprisingly, an antenna gain of –0.5 dBd is obtained under these conditions. Here, the unit dBd represents the antenna gain normalized by that of the 0.5λ dipole antenna. The high gain is a result of the appropriate choice of the ohmic resistance (R_l) on

the basis of the radiation resistance (R_r). R_l is determined from the antenna wire length and d given by Eq. (3.19). Here, because R_r is 0.24 Ω, R_l should be smaller than this value. To achieve a small ohmic resistance, d should be made as large as possible. When d is 0.8 mm, R_l is 0.25 Ω, and hence, a radiation efficiency of about 50% is achieved. This antenna gain confirms that a small rectangular NMHA in close proximity to a metal can be used in several practical applications.
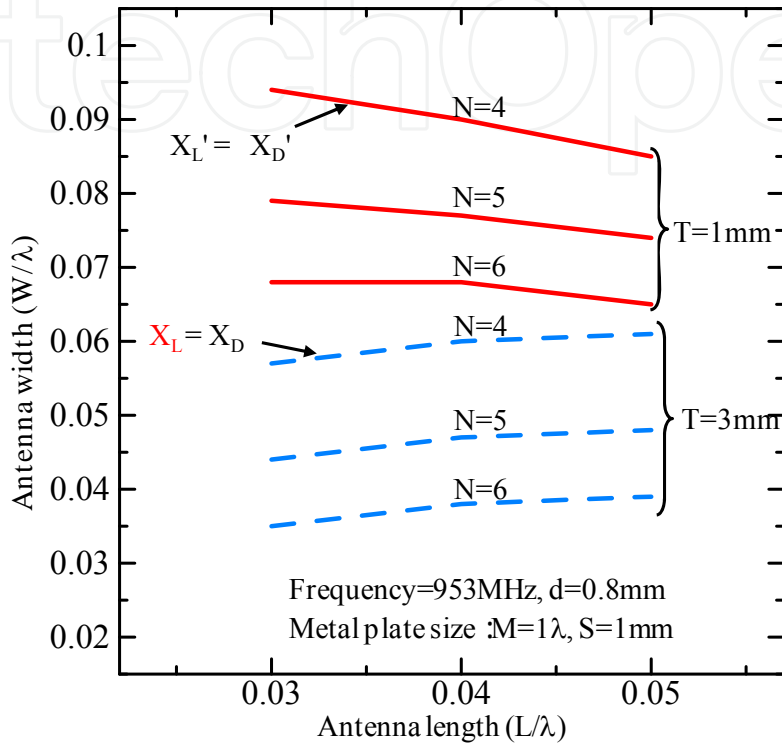

Fig. 5.2 Self-resonant structures
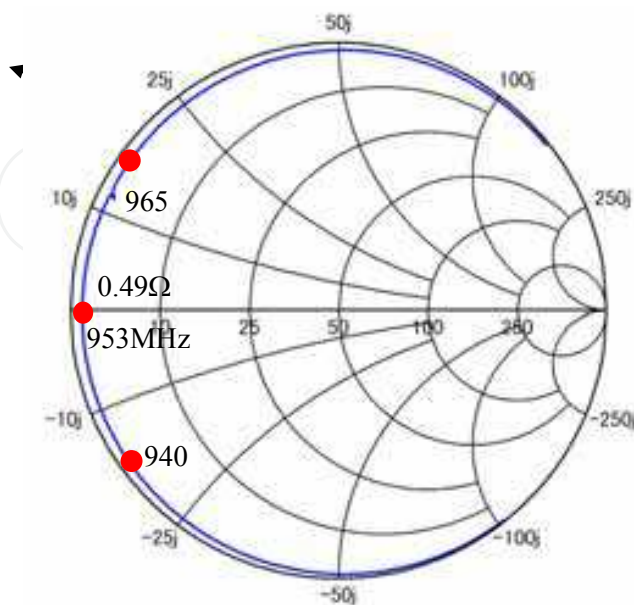
Fig. 5.3 Input impedance
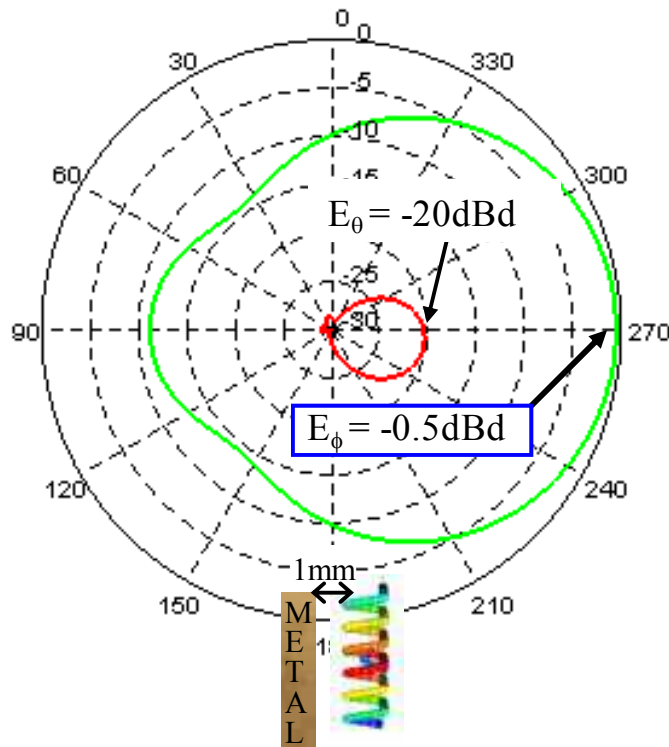
Fig. 5.4 Radiation characteristics
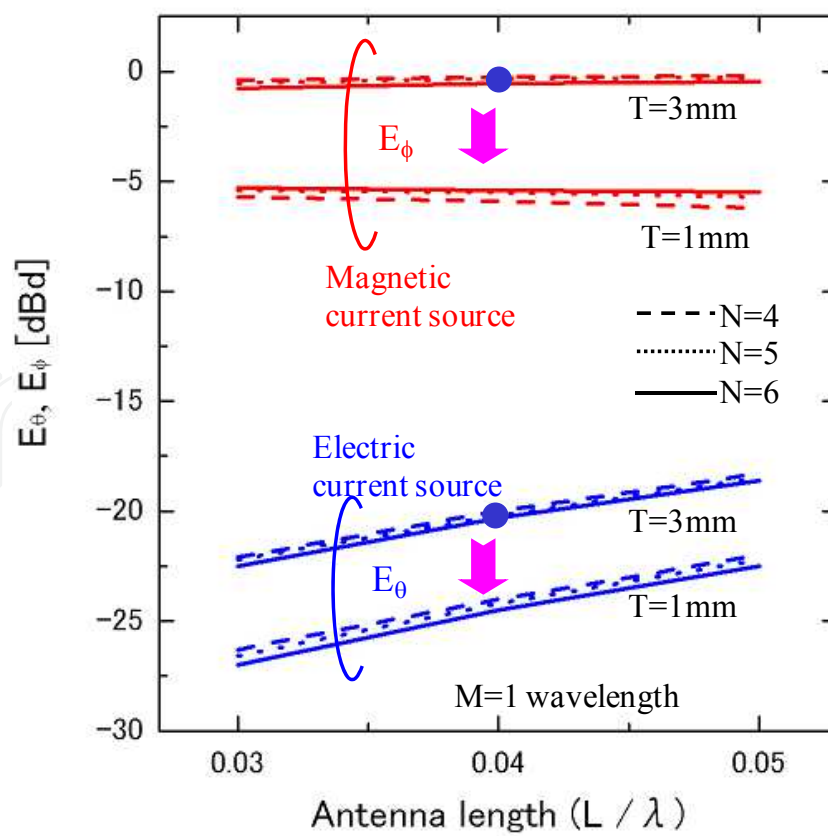
Fig. 5.5 Radiated field components

The important antenna gain characteristics for the self-resonant structures are shown in Fig. 5.5. It is noteworthy that the E_ϕ components are dominant, while the E_θ components are less than –20 dBd. There is no difference in the antenna gain even when N is changed. For large T values, a high antenna gain is achieved. When T is 3 mm, the gain is expected to be comparable to that of a 0.5λ dipole antenna. Moreover, the antenna gain remains constant for different values of L. Hence, excellent antenna gains may be obtained for small antenna sizes such as 0.03λ.

5.2 Practical antenna characteristics

A high gain can be expected for a small NMHA. However, because the input resistance of such an antenna is small, an impedance-matching structure is required for practical applications. A tap-matching structure is used for a 50-Ω coaxial cable, as shown in Figs. 5.6(a) and (b). The tap structure is rather simple. Wire diameters of 0.8 mm and 0.5 mm are selected for the antenna and the tap, respectively. Because the spacing between the antenna and the metal plate is small (1 mm), appropriate arrangement of the tap arms is important.

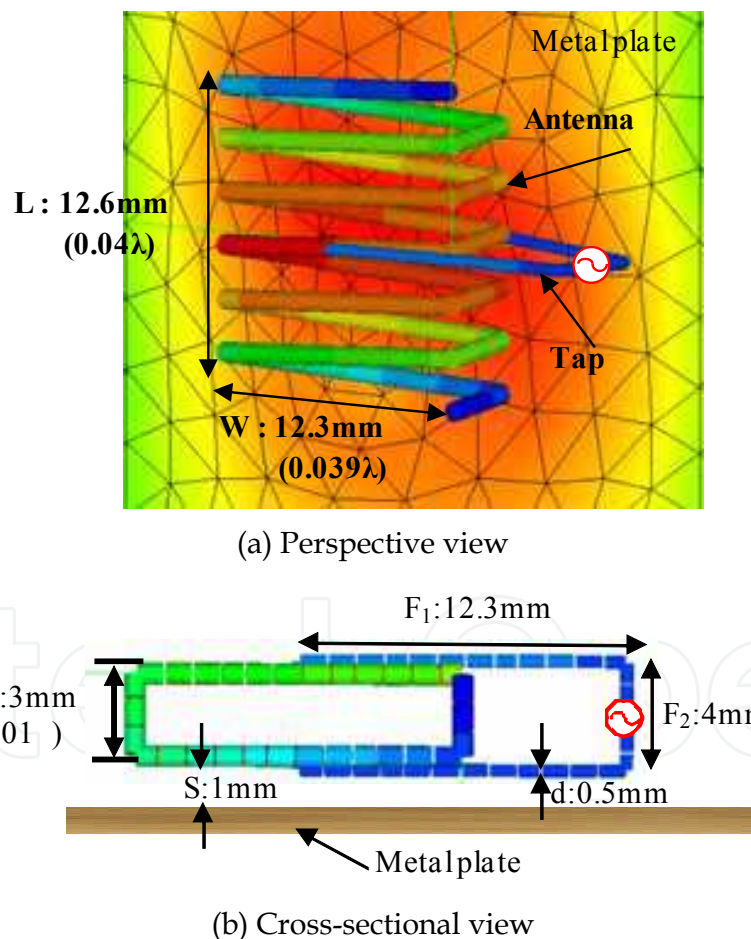(a) Perspective view

(b) Cross-sectional view

Fig. 5.6 Experimental NMHA structure

The fabricated antenna and feed cable are shown in Fig. 5.7. The tap arms are soldered to the antenna wire, and a coaxial cable is used as a feed line. A Sperrtopf balun is attached to the coaxial cable to suppress leak currents. Figure 5.8 shows the measured and calculated antenna impedances. The measured and calculated values are in good agreement, both in

the presence and absence of the tap feed. When the tap feed is used, the antenna impedance is exactly 50 Ω, and this confirms the effectiveness of the tap feed. The bandwidth characteristics are shown in Fig. 5.9. A 3.5-MHz bandwidth is obtained when VSWR < 2. This bandwidth corresponds to 0.4% of the center frequency.
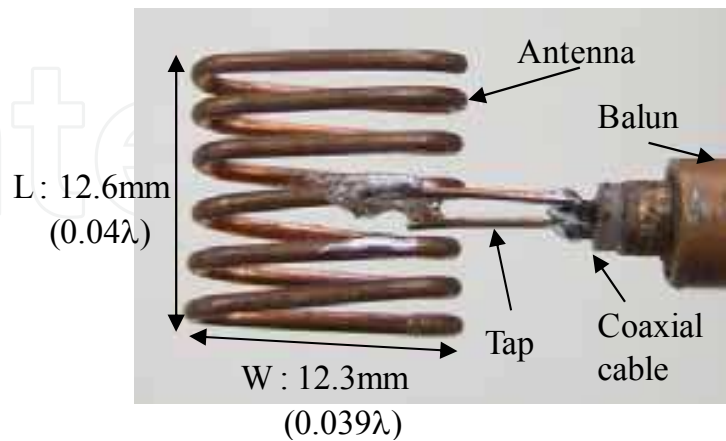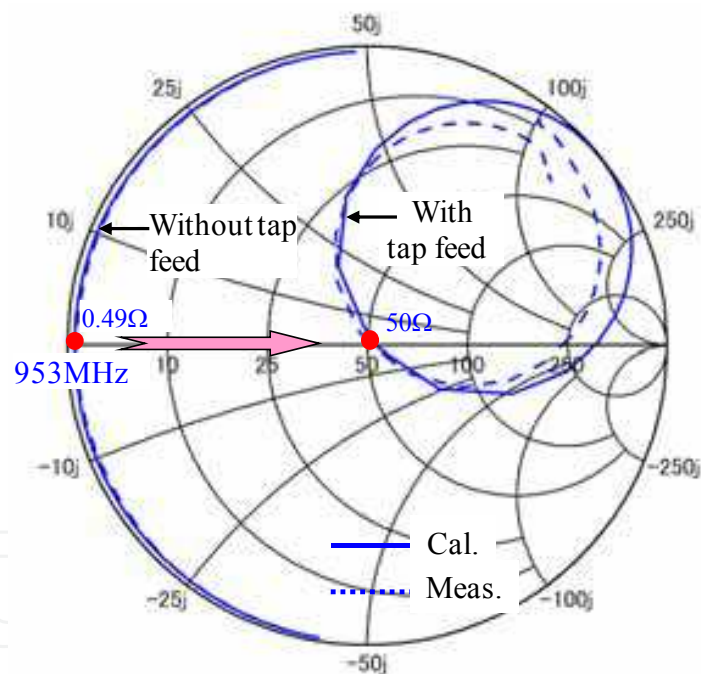

Fig. 5.7 Fabricated NMHA structure

Fig. 5.8 Input impedance

The important radiation characteristics observed when the antenna is placed near a metal plate are shown in Fig. 5.10. The separation S in this case is 1 mm. A square metal plate with a size of 0.5λ is used. The E_ϕ component is dominant when the antenna is in close proximity to the metal plate. A high antenna gain of –0.5 dBd is achieved. The E_ϕ level in the presence of the metal plate exceeds that in the absence of the metal plate by about 10 dB. The usefulness of the NMHA in a metal-proximity application is verified. At the same time, the intensity of the E_θ component decreases to –11 dBd. This shows that the electrical current source does not work well under metal-proximity conditions.

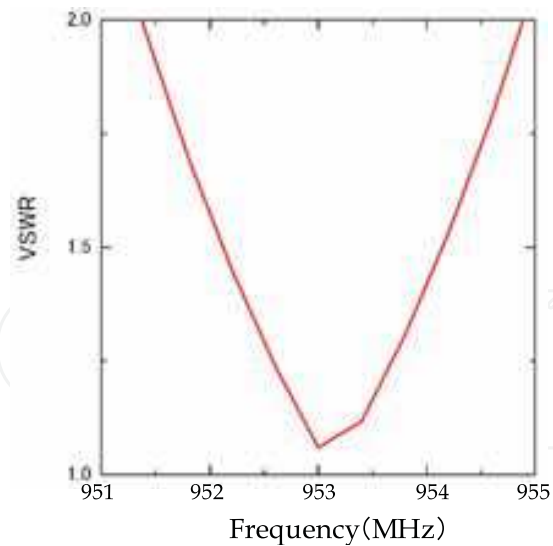Fig. 5.9 VSWR characteristics

$E_\theta = -10.1$

$E_\phi = -0.53\text{dBd}$

Cal.(dotted)

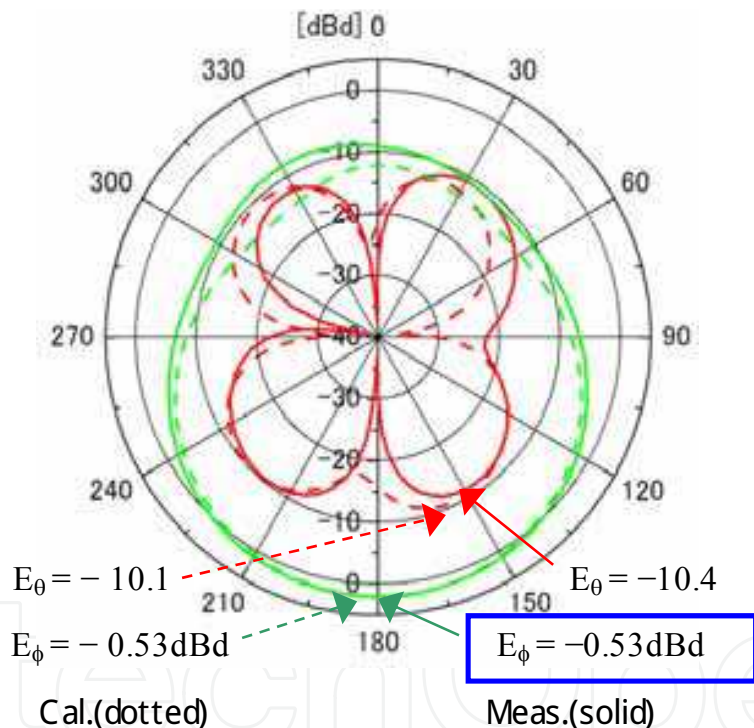$E_\theta = -10.4$

$E_\phi = -0.53\text{dBd}$

Meas.(solid)

Fig. 5.10 Radiation characteristics

5.3 RFID tag antenna

In order to use the rectangular NMHA as a tag antenna, the input impedance must be matched to the IC impedance of $Z_{IC} = 25 - j95\ \Omega$. Therefore, the antenna size and tap size are modified as shown in Fig. 5.11. The tap length is increased to obtain the necessary inductance for achieving conjugate matching with the IC capacitance. The spacing between the antenna and the metal plate is set to 1.5 mm. A 0.5λ square metal plate is used. The impedance-matching process is shown in Fig. 5.12. The tap length (T3) is important for matching the impedance to the IC. Almost complete conjugate matching can be achieved at T3 = 17 mm.

(a) Perspective view

(b) Cross-sectional view
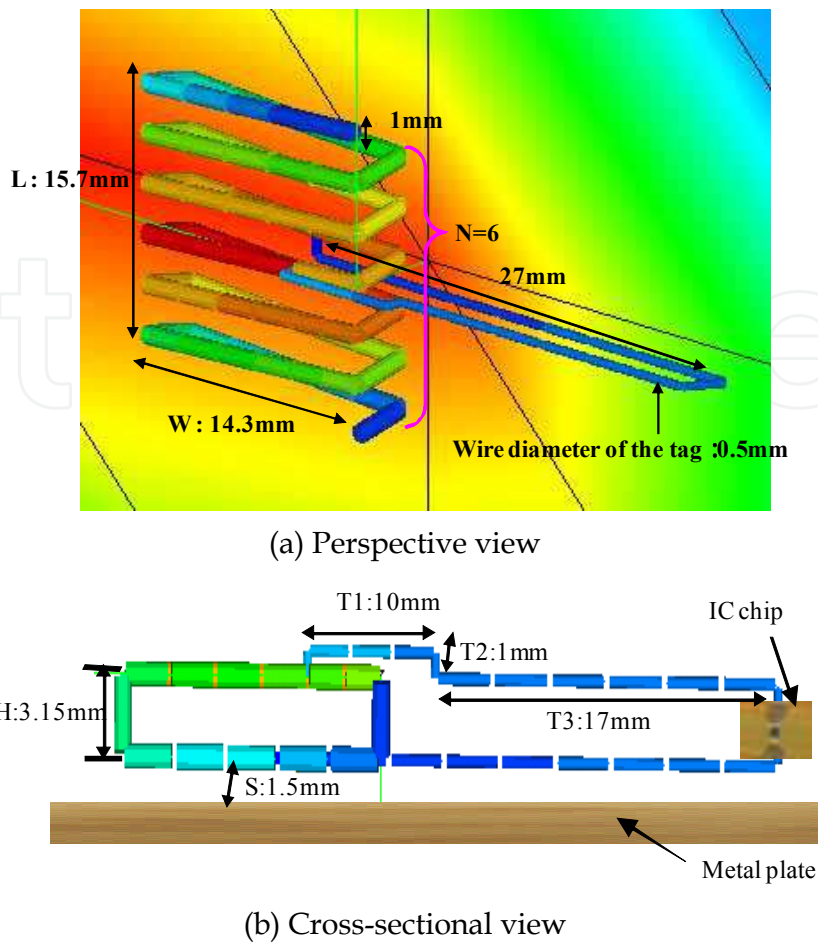
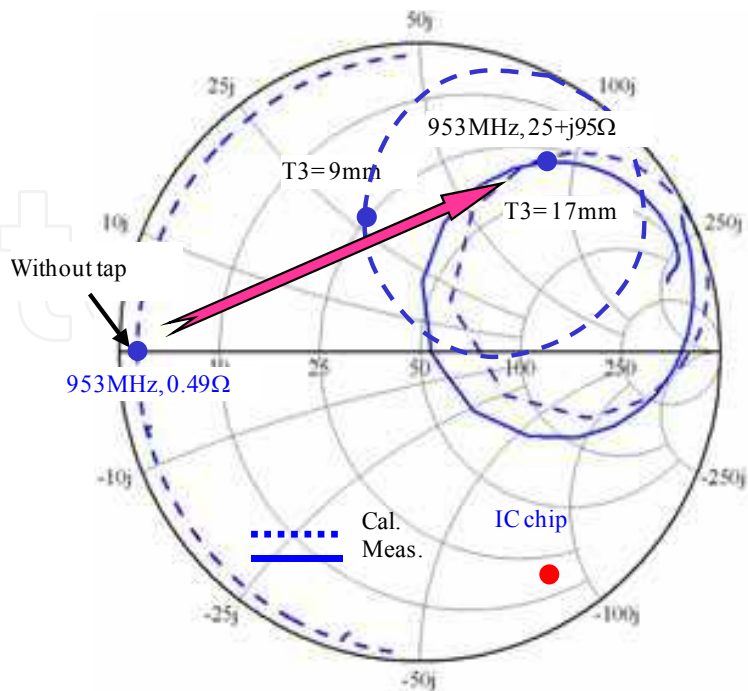Fig. 5.11 Configuration of RFID tag antenna
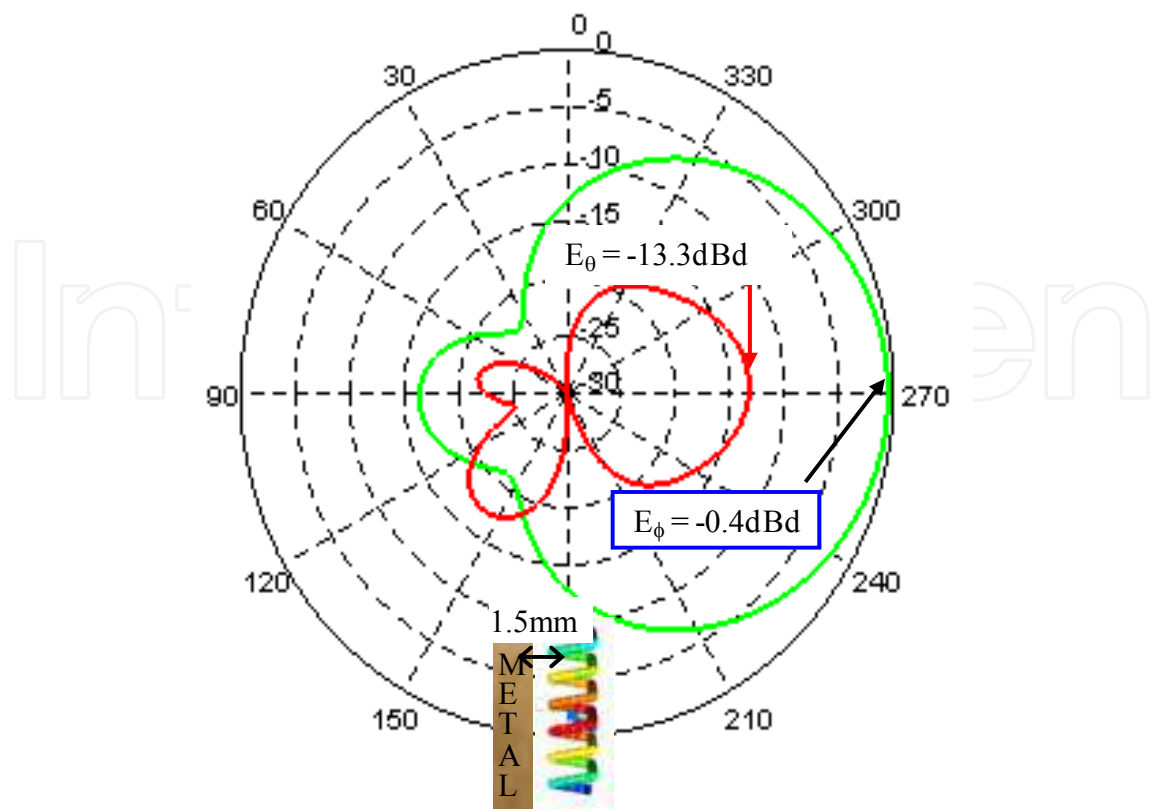

Fig. 5.12 Input impedance
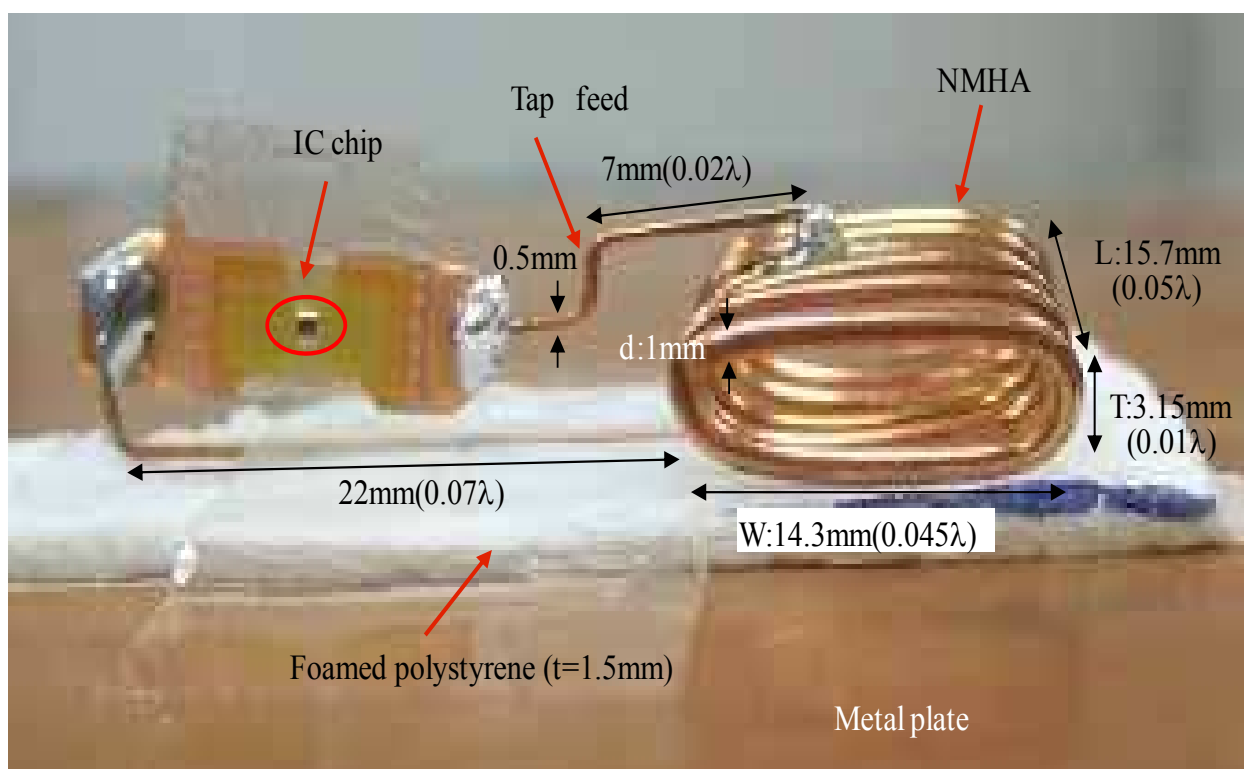
Fig. 5.13 Radiation characteristics

Fig. 5.14 Fabricated antenna

To estimate the antenna gain of this structure, we evaluate the radiation characteristics; the results are shown in Fig. 5.13. The antenna input impedance is designed to be $Z_{ANT} = 25 + j95\,\Omega$. To simplify the radiation intensity calculation, the input-impedance mismatch is ignored by adopting the "no mismatch" condition. An antenna gain of –0.4 dBd is obtained in this case. Therefore, the electrical performance is expected to be comparable to that of conventional tags.

On the basis of these results, we fabricate an actual antenna with a help of Mighty Card Corporation, as shown in Fig. 5.14. This antenna is composed of a copper wire with a diameter of 1 mm. The IC is inserted into the tap arm. The antenna and IC are placed on a piece of polystyrene foam attached to the metal plate. The thickness of the foam is 1.5 mm, and the size of the square metal plate is 0.5λ.

5.4 Read-range measurement

The read range is measured using the set-up shown in Fig. 5.15. A commercial reader antenna is used for transmitting and receiving. This reader antenna is connected to a reader unit and a computer. When the tag information is read, the tag number is shown on the computer screen. Read-range measurements are conducted by changing the distance between the reader antenna and the tag. The distance at which the tag number disappears is considered to be the read range. These read ranges might be affected by the height pattern at the measurement site, and hence, the height of the tag is so chosen that the highest possible electrical strength is obtained.
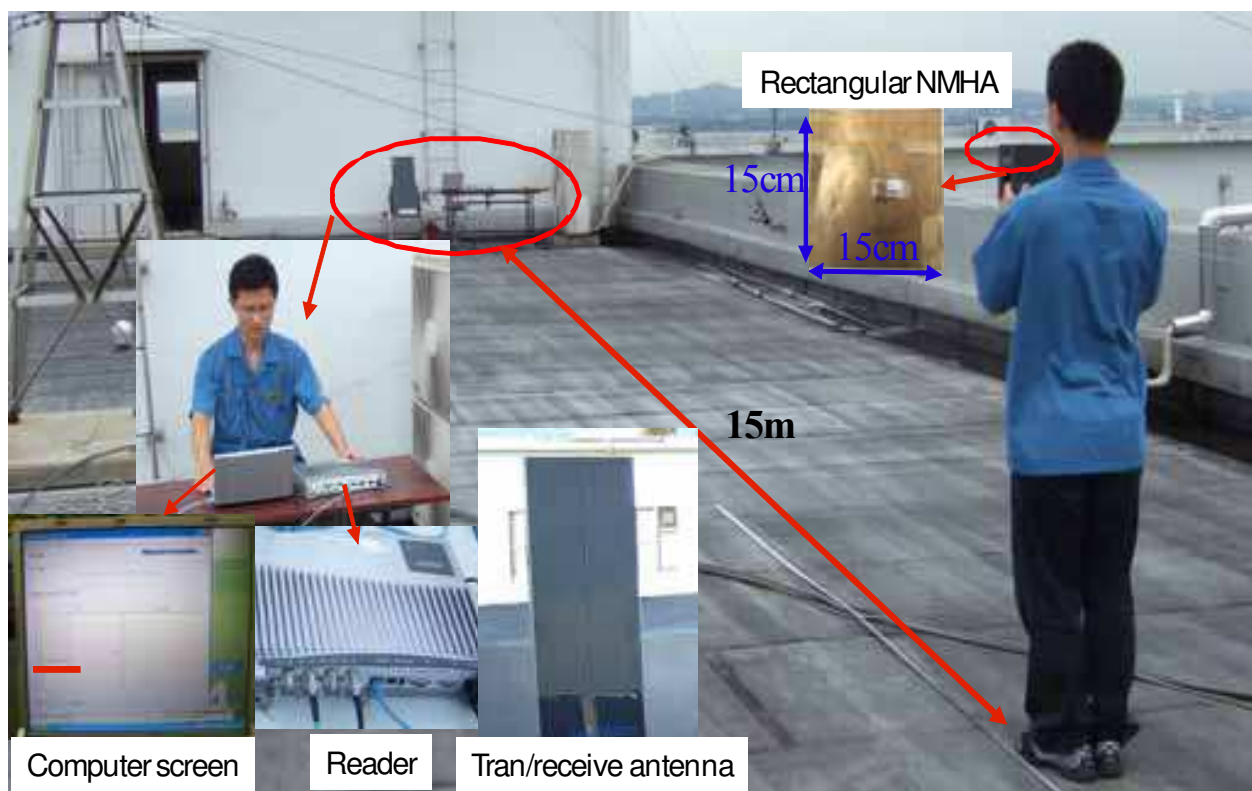

Fig. 5.15 Read-range measurement set-up

The measured read ranges are summarized in Table 5.1. For conventional antennas placed in a free space, read ranges of 9 m are obtained. In the case of a metal proximity use, read ranges become very small. For the NMHA, read ranges of 6 m and 15 m are obtained without and with the metal plate, respectively. The reason of this read range increase is attributed to the antenna gain of Fig. 5.13. The effectiveness of the tag is confirmed by the aforementioned read-range measurement.
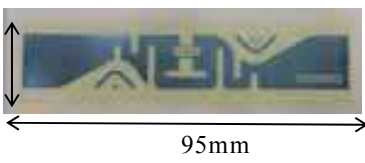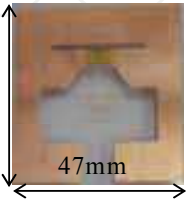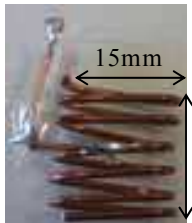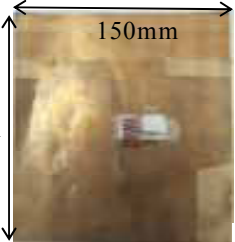
	Antenna in free space	Read range	Antenna in free space	Read range
Conventional Antenna	16mm 95mm	9m	42mm 47mm	9m
	Without a metal plate	Read range	With a metal plate	Read range
Low profile NMHA	15mm 15mm	6m	150mm 150mm	15m

Table 5.1 Results of read-range measurement

6. Conclusions

A normal-mode helical antenna (NMHA) with a small size and high gain is proposed for use as an RFID tag antenna under metal-plate proximity conditions. The important features of the design are as follows:

1. Fundamental equations for important electrical characteristics have been summarized, and useful databases have been shown.
2. The antenna efficiency, which is related to the structural parameters, is important for achieving high antenna gain.
3. A simple design equation for determining the self-resonant structures has been developed.
4. For the fabrication of an actual antenna, the tap feed has been carefully designed so that a small input resistance is obtained.
5. A simple design equation for determining the tap-feed structures has been developed.
6. A small RFID tag antenna that can be used under metal-plate proximity conditions has been designed.
7. A read range superior to that of conventional tags has been achieved.

7. References

[1] http://www.alientechnology.com/tags/index.php

[2] http://www.omni-id.com/products/omni-id-max.php

[3] Xuezhi Zeng, et al, "Slots in Metallic Label as RFID Tag Antenna," APS 2007, pp.1749-1752, Hawaii, June.2007.

[4] W.G. Hong, W.H. Jung and Y. Yamada, "High Performance Normal Mode Helical Antenna for RFID Tags", IEEE AP-S'07, pp.6023-6026, Hawaii, June 2007

[5] K. Tanoshita, K. Nakatani and Y. Yamada, "Electric Field Simulations around a Car of the Tire Pressure Monitoring System", IEICE Trans. Commu., Vol.E90-B, No.9, 2416-2422, 2007

[6] W. G. Hong, Y. Yamada and N. Michishita, Low profile small normal mode helical antenna achieving long communication distance ", Proceedings of iWAT2008, pp.167-170, March 2008

[7] Q.D. Nguyen, N. Michishita, Y. Yamada and K. Nakatani, "Electrical Characteristics of a Very Small Normal Mode Helical Antenna Mounted on a Wheel in the TPMS Application", IEEE AP-S'09, Session 426, No.4, June 2009

[8] J. D. Kraus, "ANTENNAS, second edition", McGraw-Hill Book Company, pp. 333-338, 1988

[9] H.A. Wheeler, "Simple Inductance formulas for Radio Coils," Proc.IRE, Vol.16, pp.1398-1400, 1928.

[10] W. L. Stutzman and G. A. Thiele, "Antenna Theory and Design, second edition", John Wiley & Sons, Inc., pp. 43-47 and p.71, 1998

[11] W. L. Stutzman and G. A. Thiele, "Antenna Theory and Design, second edition", John Wiley & Sons, Inc., pp.71-75, 1998

[12] Q.D. Nguyen, N. Michishita, Y. Yamada and K. Nakatani, "Deterministic Equation for Self-Resonant Structures of Very Small Normal-Mode Helical Antennas", IEICE Trans. Communications., to be published in May, 2011

[13] J. S. McLean, "A re-examination of the fundamental limits on the radiation Q of electrically small antenna", IEEE Trans. Antennas Propag., Vol.44, No.5, pp.672-676, May 1996

[14] Q.D. Nguyen, N. Michishita, Y.Yamada and K. Nakatani, "Design method of a tap feed for a very small no-mal mode helical antenna", IEICE Trans. Communications., to be published in Feb., 2011

[15] K. Fujimoto, A. Henderson, K. Hirasawa and J.R. James, "SMALL ANTENNAS", Research Studies Press Ltd., pp.86-92,1987

[16] K. Fujimoto, A. Henderson, K. Hirasawa and J.R. James, "SMALL ANTENNAS", Research Studies Press Ltd., pp.78,1987

[17] Simon Ramo, John R. Whinnery and Theodore Van Duzer, FIELDS AND WAVES IN COMMUNICATION ELECTRONICS – Third Edition, JOHN WILEY&SONS, INC., pp.189-193, 1993

[18] W. L. Stutzman and G. A. Thiele, "Antenna Theory and Design, second edition", John Wiley & Sons, Inc., p.75, 1998

[19] http://www.mightycard.co.jp/

[20] W.G. Hong, N. Michishita and Y. Yamada, "Low-profile Normal-Mode Helical Antenna for Use in Proximity to Metal", ACES Journal, Vol.25, No.3, pp.190-198, March 2010
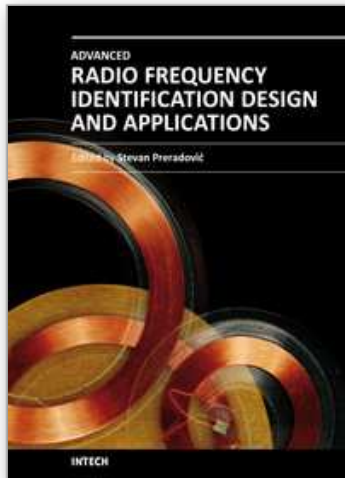
Advanced Radio Frequency Identification Design and Applications

Edited by Dr Stevan Preradovic

Radio Frequency Identification (RFID) is a modern wireless data transmission and reception technique for applications including automatic identification, asset tracking and security surveillance. This book focuses on the advances in RFID tag antenna and ASIC design, novel chipless RFID tag design, security protocol enhancements along with some novel applications of RFID.

How to reference

In order to correctly reference this scholarly work, feel free to copy and paste the following:

Yoshihide Yamada (2011). Design of a Very Small Antenna for Metal-Proximity Applications, Advanced Radio Frequency Identification Design and Applications, Dr Stevan Preradovic (Ed.), ISBN: 978-953-307-168-8, InTech, Available from: http://www.intechopen.com/books/advanced-radio-frequency-identification-design-and-applications/design-of-a-very-small-antenna-for-metal-proximity-applications

INTECH
open science | open minds